

# Groups, field and isolated early-type galaxies

## I. Observations and nuclear data

G. Denicolo,<sup>1?</sup> Roberto Terlevich,<sup>2Y</sup> Elena Terlevich,<sup>2Y</sup> Duncan A. Forbes,<sup>3</sup>  
Alejandro Terlevich,<sup>4</sup> Luis Carrasco<sup>2</sup>

<sup>1</sup> Institute of Astronomy, Madingley Road, Cambridge, CB3 0HA, United Kingdom

<sup>2</sup> Instituto Nacional de Astrofísica, Óptica y Electrónica, Tonantzintla, Puebla, México

<sup>3</sup> Centre for Astrophysics & Supercomputing, Swinburne University, Hawthorn, VIC 3122, Australia

<sup>4</sup> School of Physics and Astronomy, University of Birmingham, Edgbaston, Birmingham, B15 2TT, United Kingdom

Accepted November 3rd 2004 Received; in original form July 2004

### ABSTRACT

This is the first paper of a series on the investigation of stellar population properties and galaxy evolution of an observationally homogeneous sample of early-type galaxies in groups, field and isolated galaxies.

Here we present high signal-to-noise long-slit spectroscopy of 86 nearby elliptical and S0 galaxies. Eight of them are isolated, selected according to a rigorous criterion, which guarantees a genuine low-density subsample. The present survey has the advantage of covering a larger wavelength range than normally found in the literature, which includes [O III] 5007 and H $\alpha$ , both lines important for emission correction. Among the 86 galaxies with S/N > 15 (per resolution element, for r<sub>e</sub>/8 central aperture), 57 have their H $\alpha$ -index corrected for emission, the average correction is 0.190 Å in H $\alpha$ ; 42 galaxies reveal [O III] 5007 emission, of which 16 also show obvious H $\alpha$  emission. Most of the galaxies in the sample do not show obvious signs of disturbances nor tidal features in the morphologies, although 11 belong to the Arp catalogue of peculiar galaxies; only three of them (NGC 750, NGC 751, NGC 3226) seem to be strongly interacting. We present the measurement of 25 central line-strength indices calibrated to the Lick/IDS system. Kinematic information is obtained for the sample. We analyse the line-strength index vs velocity dispersion relations for our sample of mainly low density environment galaxies, and compare the slope of the relations with cluster galaxies from the literature. Our main findings are that the index- $\sigma_0$  relations presented for low-density regions are not significantly different from those of cluster E/S0s. The slope of the index- $\sigma_0$  relations does not seem to change for early-type galaxies of different environmental densities, but the scatter of the relations seems larger for group, field and isolated galaxies than for cluster galaxies.

**Keywords:** galaxies: stellar content { galaxies: abundances { galaxies: elliptical and lenticular { galaxies: nuclei { galaxies: kinematics and dynamics

### 1 INTRODUCTION

The standard paradigm for galaxy formation is one of hierarchical clustering and subsequent merging to form progressively larger galaxies (White & Rees 1978). All galaxies are located within dark matter halos, and the properties of galaxies depend on the assembly history of these dark matter

halos and hence their environment. This process has been modelled by semi-analytical methods (e.g. Baugh et al. 1998; Kauffmann et al. 1999; Somerville & Primack 1999) and by hydrodynamical simulations (e.g. Cen & Ostriker 1992; Pearce et al. 1999; Berlind et al. 2003). For example, Kauffmann & Charlot (1998) predict that galaxies in low density environments are younger (in a luminosity weighted sense) on average than those in clusters as they have a more extended merger history. They also predict that massive ellipticals are younger than smaller ones, again due to merger-induced star formation. Quantitative predictions depend on

? Visiting at INAOE, México.

Y Visiting Fellow, IoA, Cambridge. Email for contact: rjt@inaoep.mx and terlevic@inaoep.mx

the details of the gas physics and feedback processes (e.g. Kau et al. 2002; Kau man et al. 2004). High quality data already exists for the cluster ellipticals, thus determining the ages and metallicities of field and group ellipticals is a key test of the HCM paradigm (Gonzalez 1993; Bower et al. 1998; Trager et al. 2000a,b; Kuntschner 2000; Terlevich & Forbes 2002; Chiosi & Camaro 2002; Kuntschner et al. 2002; Willis et al. 2002).

In an effort to disentangle the degeneracy of age and metallicity effects on the gross properties of stellar populations, Worthey (1994, 1997) developed a series of stellar population spectral synthesis models. He showed that certain predominantly age (i.e. H, H<sub>α</sub>) and metallicity (i.e. Fe, Mg/Fe) sensitive spectral absorption features can break the degeneracy, and the luminosity weighted mean ages and metallicities can be determined. In a study of bright galaxies in the Fornax cluster, Kuntschner & Davies (1998) showed that, as predicted by the high  $z$  studies, the cluster ellipticals are indeed uniformly old, and span a range in metallicities. However, earlier studies of field (and loose group) ellipticals (Gonzalez 1993; Trager 1997) seem to show just the opposite, displaying a uniform metallicity, but spanning a range in ages. This suggests the possibility of an environmental dependence of the colour-magnitude relation (CMR), or maybe two different mechanisms operating in cluster and field environments, conspiring to produce similar CMRs. The universality of the CMR from cluster core to the field environments, and its interpretation as a metallicity sequence, is fundamental to its placing a limit on the formation epoch of cluster elliptical galaxies to  $z > 1$  (e.g. Bower, Lucey & Ellis 1992). If there is in fact a conspiracy between age and metallicity producing a tight CMR, this limit could be significantly loosened.

We have carried out a large and observationally homogeneous survey of local early-type galaxies in low density environments with the aim of determining nuclear parameters, kinematic, age and metallicity gradients. This will help to infer whether the central values represent a small localised starburst or whether the whole galaxy was involved. The spectra, when combined with existing photometry, will allow us to investigate scaling relations such as the fundamental plane, Mg- and colour-magnitude relations for field galaxies, and directly compare how these relations agree with galaxy formation histories, from their mean ages and metallicities. The luminosity weighted mean ages and metallicities of these galaxies will also allow us to directly test fundamental predictions of hierarchical models for structure formation in the universe. The emission line data will allow the discrimination among the different ionization mechanisms and provide information about the kinematical status of the ionized gas. In this paper we present the data, central measures and comparisons with previous work.

The paper is divided as follows. In Section 2 we describe the sample selection, and Section 3 details the observations and data reduction procedures. Section 4 describes the transformation of spectral index measurements to the Lick/IDS system, an improved method for emission correction of the Balmer line indices, and the derivation of errors from repeated measurements. We explain the determination of kinematical properties and errors in Section 5. Section 6 presents the finally corrected line-strength indices. In Section 7 we analyse the index vs central velocity dispersion

relations. Our results are summarized in Section 8. Complementary information about the sample and fully corrected Lick indices are presented in Appendices A and B.

## 2 SELECTION OF GALAXIES

We have selected early-type galaxies that lie in relatively low density environments, i.e., in loose groups (56), the general field (19) and truly isolated galaxies (8). However, we also observed 3 Virgo cluster galaxies, to complete a total of 86 galaxies. The objects are distributed all over the sky but with strong concentrations around the galactic poles and away from the galactic plane. Galaxies in groups come from the group catalogue of Garcia (1993).

Eight galaxies were classified as truly isolated by Reda et al. (2004). Below, we describe briefly how isolated galaxies were selected. By using the Lyon-Madeleine Extragalactic Data Archive (LEDA) of 100,000 galaxies, the following criteria were applied:

Morphological type T 6–3  
Virgo corrected recession velocity  $V \leq 9000 \text{ km s}^{-1}$ ,  
Apparent magnitude  $B_T \leq 14.0$ .

This produced 330 galaxies which could be considered as potential isolated galaxies. The galaxies were compared to the rest of the catalogue and accepted as being isolated if they had no neighbours which were:

within  $700 \text{ km s}^{-1}$  in recession velocity,  
within  $0.67 \text{ Mpc}$  in the plane of the sky (assuming  $H_0 = 75 \text{ km s}^{-1} \text{ Mpc}^{-1}$ ),  
less than 2 magnitudes fainter in  $B_T$ .

Lastly, in the process of determining isolated objects, all galaxies were checked visually on the Digitized Sky Survey (DSS) images to ensure no near projected galaxy. This produced a final list of 40 early-type isolated galaxies; in this work we have obtained spectra of 8 of them.

By exclusion, non-cluster galaxies which are not associated with groups and also not identified as isolated galaxies are then assumed to lie in the general field.

The Tully (1987) local density parameter is available for about 3/4 of our sample. Values range from 0.08 (isolated) to 3.99 (a Virgo galaxy). The sample also shows a good overlap with the Lick/IDS system, with 59 galaxies in common (Trager et al. 1998).

## 3 OBSERVATIONS AND DATA REDUCTION

Long-slit spectra have been obtained, during five different runs, accounting for a total of 30 nights, at the 2.12 m telescope of Observatorio Astronómico Guillermo Haro (OAGH), in Cananea, Mexico. The telescope is equipped with a Boller & Chivens spectrograph and a Tek 1024 pix<sup>2</sup> CCD camera. Parameters of the observations are reported in Table 1. We have obtained spectra in two wavelength ranges (blue and red), covering a total range from 3850 Å to 6700 Å. Two 300 lines mm<sup>-1</sup> grating blazed at 4650 Å and 5900 Å (for the blue and red wavelength ranges, respectively) yielded a dispersion of 65 Å mm<sup>-1</sup> on the spectrograph CCD, i.e.,

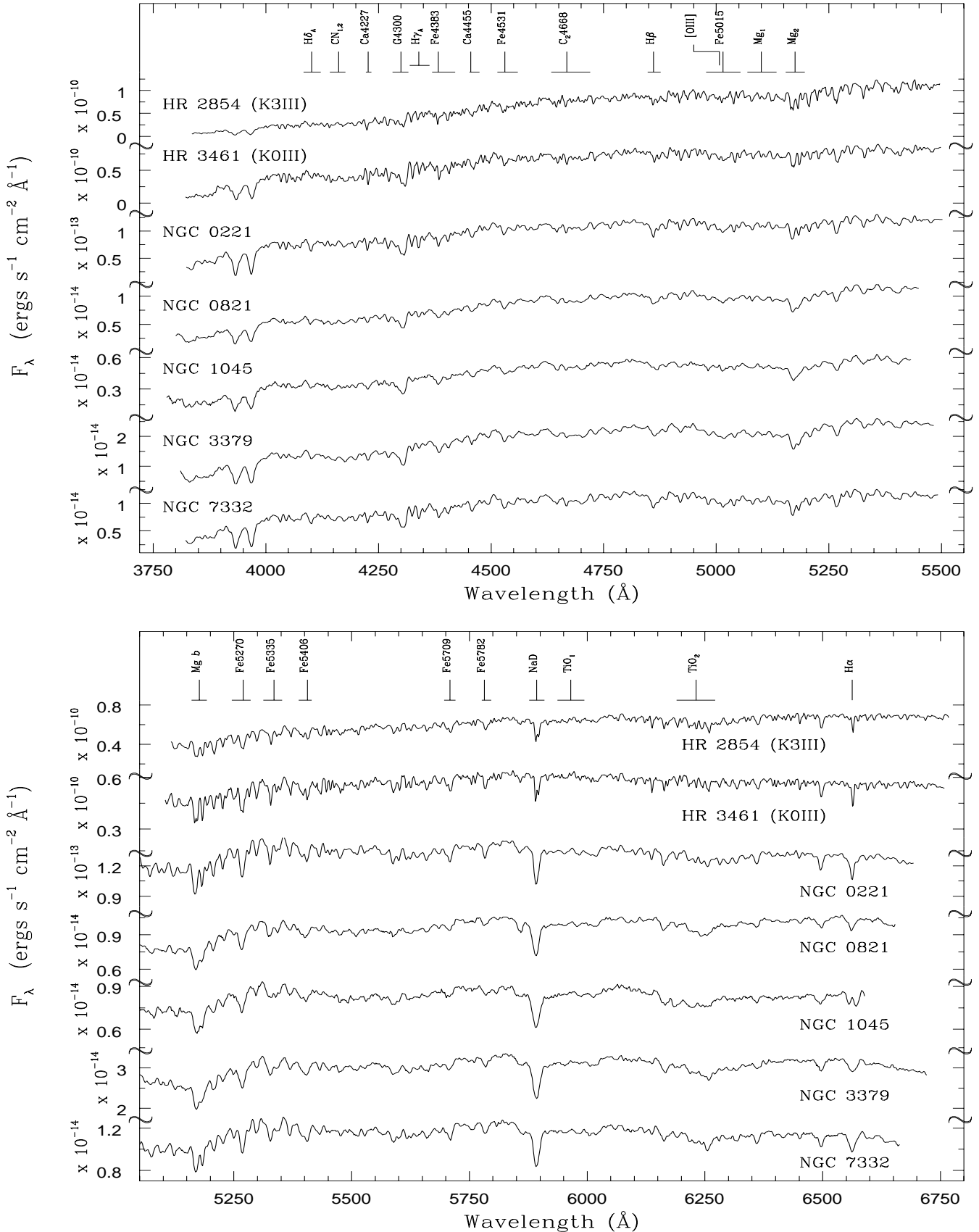


Figure 1. Typical spectra of two stars and five galaxies. The top panel shows the spectra in the blue wavelength range, the bottom panel presents the red wavelength range. All spectra are flux calibrated using standard Oke (1990) stars. The galaxy spectra are redshift corrected and represent the nuclear  $r_e/8$  extraction.

an instrumental dispersion of  $1.6 \text{ \AA/pixel}$ . Typically, exposure times were between 300 to 1200 seconds per galaxy frame. Total exposure times were chosen to obtain  $S/N > 40$  per  $\text{\AA}$  at  $5000\text{\AA}$ . The slit has been centred on the nucleus and oriented along the major axis for most of the galaxies. We observed the galaxies close to minimum zenithal distance in order to minimize differential refraction effects. Some neighbouring galaxies have been observed along the line connecting their nuclei. Instrumental resolution of  $6 \text{ \AA}$  (FWHM) was achieved with a slit width of  $1.5 \text{ arcsec}$ . Table 2 presents the detailed listing of the galaxy observations. The seeing was generally better than  $2.0 \text{ arcsec}$ . Additionally we observed 46 different standard stars (mainly K-giants) to be used as templates for velocity dispersion measurements, and for calibration of the line-strength indices to the Lick/IDS system (Gonzalez 1993). Six spectrophotometric standard stars were also taken to enable flux calibration. At least two different spectrophotometric standard stars were observed per night. Table 3 lists all observed stars with their spectral types (obtained from SIMBAD, operated by CDS, Strasbourg). In addition, a bona de elliptical galaxy, NGC 3379, was observed in every run to serve as a link galaxy for the measurement of indices and velocity dispersion between the different observing runs.

All data reduction was performed using packages in IRAF. Each frame has been treated separately. Initial reduction of the CCD frames involved overscan correction, bias subtraction, the removal of pixel-to-pixel sensitivity variations (using dome flat exposures), and correction for uneven illumination along the slit (using twilight sky exposures). Careful wavelength calibration was performed using H $\alpha$ -Ar or Fe-Ar lamps. For the blue wavelength range observations ( $3850\text{-}5450 \text{ \AA}$ ), H $\alpha$ -Ar lamps were taken before and after each exposure to achieve an accurate wavelength calibration. For the red wavelength range ( $5100\text{-}6700 \text{ \AA}$ ), we followed the same procedure using Fe-Ar lamps. A linear fit between pixel number and wavelength for  $30 \text{ arc}$  lines gave an rms calibration error  $< 0.1 \text{ \AA}$  in most cases. The galaxy frames were then corrected for atmospheric extinction, and afterwards, the continuum shape of the spectra was corrected to a relative flux scale with the help of the spectrophotometric standard stars. The cosmic rays were cleaned with the task crmedian, which detects cosmic rays from pixels deviating by a 3-sigma level from the median at each pixel. Sky subtraction was then performed in each frame and finally, we used the task apall to extract 1D-spectra. We have extracted the central  $r_e/8$  ( $r_e$  is the effective radius<sup>y</sup>) from all galaxy frames, and these extractions will be used as our standard nuclear observations. A sample of seven typical spectra is shown in Figure 1.

The signal-to-noise ratio ( $S/N$ ) per resolution element (resolution element =  $6 \text{ \AA FWHM}$ ) of individual 1-D galaxy extractions ranges from 9 to about 100. The signal-to-noise was estimated assuming Poisson statistics,  $\sqrt{N}$ , where  $N$  is the number of photon counts. The gain of the CCD, as presented in Table 1, is  $1.85 \text{ e}^-/\text{ADU}$ , and therefore the mean number of counts in the spectra was multiplied by the gain to obtain the photon statistics. The  $S/N$  measurement was performed in regions of  $120 \text{ \AA}$  encompassing the continua

<sup>y</sup> Effective radii are from Trager et al. 2000b and RC3.

Table 1. Instrumental set-up.

Telescope	OAGH 2.12 m, Cananea, Mexico	
	Blue	Red
Spectral range [ \AA ]	3850-5450	5100-6700
Date of observations	2000 Mar 25-29 2000 Apr 01-02 2000 Oct 20-26 2001 Oct 13,18-19 2002 Apr 08	2000 Mar 30-31 2000 Apr 03 2001 Mar 27-29 2001 Oct 14-17 2002 Apr 06-07
Spectrograph	B & C	B & C
Detector	CCD Tek 1024	CCD Tek 1024
Gain [ e^- /ADU ]	1.85	1.85
Read-out-noise [ e^- rms ]	3.7	3.7
Pixel size [ m^2 ]	24	24
Spatial scale [ \textcircled{m}/pixel ]	0.44	0.44
Slit length [ \textcircled{m} ]	3	3
Slit width [ \textcircled{m} ]	1.5	1.5
G rating [ lines/mm ]	300	300
Dispersion [ \textcircled{m}/pixel ]	1.6	1.6
Resolution [ \textcircled{m} ]	6	6
Seeing [ arcsec ]	1.5 - 2	1.5 - 2

of  $Mg_2$  index or the continua of  $TiO_2$  index, for the blue or red spectra, respectively.

We have only performed equivalent width measurements in spectra with  $S/N > 15$  per resolution element. We opted to work with the galaxy frames separately to avoid any possible wavelength mismatch when combining the frames. This decision offers statistical advantages as we are working with  $\sim 700$  spectral frames of  $S/N > 15$  (per resolution element) for a sample consisting of a total of 86 different galaxies (total of 8 frames/galaxy on average, where 4 frames are in the red wavelength range and 4 frames in the blue spectral range, in general). The line-strength index measurements were therefore performed in all spectra separately and later averaged for each galaxy.

The median  $S/N$  per frame is  $\sim 40$  per resolution element (Figure 2). The effective  $S/N$  per galaxy can then be estimated as, approximately, the square-root of the number of frames per galaxy times the median  $S/N$  per frame, i.e., effective  $S/N$  per galaxy in the blue or red spectral range (average of 4 frames per galaxy per spectral range)  $\sqrt{\frac{P}{4}} \sim 40 \sqrt{80}$  per resolution element.

Finally, we refer to the data in this paper as the OAGH sample.

#### 4 LICK INDICES

Absorption line indices in the visual as defined by the Lick group (e.g.,  $H\beta$ ,  $Mg_2$ , Fe5270, Fe5335, etc, Burstein et al. 1984; Faber et al. 1985) have proven to be a useful tool for the derivation of ages and metallicities of unresolved stellar populations.

Our spectra cover the 21 Lick indices defined in Faber et al. (1985) and Worthey et al. (1994), and the subsequent four Balmer indices ( $H_{\alpha,F}$ ,  $H_{\beta,F}$ ) first presented in Worthey & Ottaviani (1997). The indices are calculated by the standard equations:

Table 2. Log of observations: galaxies.

Galaxy	Classification	B <sub>T</sub> [mag]	Exp. [sec]	PA [°]	Galaxy	Classification	B <sub>T</sub> [mag]	Exp. [sec]	PA [°]		
		Blue	Red				Blue	Red			
ESO 462-G 015	E 3	12.95	3600	6300	166	NGC 3599	SA 0	12.82	9600	3600	20
MCG -01-02-018	(R')SA (r)0	14.23	3600	3600	170	NGC 3607	SA 0	10.82	2700	2700	120
NGC 0016	SA B 0	13.00	3600	2700	20	NGC 3608	E 2	11.70	3600	2700	75
NGC 0221	cE 2	9.03	3600	2700	90	NGC 3610	E 5	11.70	3600	3600	130
NGC 0315	E + LINER-Sy1	12.20	5400	2700	55	NGC 3613	E 6	11.82	3600	1800	102
NGC 0474	SA (s)0	12.37	4800	2700	90	NGC 3636	E 0	12.82	4800	2400	90
NGC 0584	E 4	11.44	3600	2700	55	NGC 3640	E 3	11.36	3600	2400	100
NGC 0720	E 5	11.16	2700	2700	140	NGC 3665	SA (s)0	11.77	3600	1800	130
NGC 0750	E pec	12.89	4800	3600	166	NGC 3923	E 4-5	10.80	1200	2700	45
NGC 0751	E pec	13.50	4800	3600	166			1200			90
NGC 0777	E 1	12.49	3600	4800	155	NGC 3941	SB (s)0 Sy2	11.25	3600	1800	90
NGC 0821	E 6	11.67	2700	2700	32	NGC 4125	E 6 pec LINER	10.65	4800	1800	80
NGC 0890	SA B (r)0	12.20	3600	2700	140	NGC 4261	E 2-3 LINER	11.41	3600	900	90
NGC 1045	SA 0 pec	13.52	3600	2700	40	NGC 4365	E 3	10.52	3600	2700	40
NGC 1052	E 4 LINER-Sy2	12.08	2700	2700	122	NGC 4374	E 1 LINER	10.09	1800	900	90
NGC 1132	E	13.25	3600	6300	140	NGC 4494	E 1-2	10.71	3600	1800	180
NGC 1407	E 0	10.70	2700	1800	180			1800			90
NGC 1453	E 2-3	12.77	3600	2700	45	NGC 4550	SB 0	12.56	3600	1800	90
NGC 1600	E 3	11.93	3600	2700	15			1200			35
NGC 1700	E 4	12.20	2400	6300	90	NGC 4754	SB (r)0	11.52	3600	1800	115
NGC 1726	SA (s)0	12.66	4500	5100	180	NGC 5322	E 3-4 LINER	11.14	4800	3600	95
NGC 2128	S0	13.60	8400	7200	140	NGC 5353	S0	11.96	4800	4800	180
NGC 2300	SA 0	12.07	9900	9900	180	NGC 5354	SA 0 LINER	12.33	4800	3600	90
NGC 2418	E	13.16	7500	6600	50	NGC 5363	IO LINER	11.05	5400	2700	135
			2700		35	NGC 5444	E +	12.78	4800	2400	67
NGC 2513	E	12.59	8400	3600	90	NGC 5557	E 1	11.92	3600	1800	90
NGC 2549	SA (r)	12.19	3600	1800	90	NGC 5576	E 3	11.85	3600	1800	90
NGC 2768	S0 LINER	10.84	3600	1800		NGC 5638	E 1	12.14	3600	1800	170
			2700		90	NGC 5812	E 0	12.19	4800	2400	90
NGC 2872	E 2	12.86	4800	2400	110	NGC 5813	E 1-2	11.45	7200	5400	145
NGC 2911	SA 0 pec sy	12.50	6000	9300	50	NGC 5831	E 3	12.45	6000	2400	90
NGC 2974	E 4	12.30	3600	2400	135	NGC 5845	E :	13.50	8400	2400	120
NGC 3091	E 3	12.13	2700	1800	90	NGC 5846	E 0-1 LINER-H II	11.05	7200	4500	180
NGC 3098	S0	12.89	6000	3600	180			1800			90
NGC 3115	S0	9.87	2700	2280	135	NGC 5846A	cE 2-3	14.10	7200	4500	180
NGC 3139	S0 pec	15.00	2700	1800	90	NGC 5854	SB (s)0	12.71	4800	3600	155
NGC 3156	S0	13.07	4800	2700	40	NGC 5864	SB (s)0	12.77	3600	2400	155
NGC 3193	E 2	11.83	3600	2700	90	NGC 5869	S0:	12.91	2700	1800	120
NGC 3226	E 2 pec LINER	12.30	4800	2400	90	NGC 5982	E 3	12.04	3600	1800	114
NGC 3245	SA (r)0 H II-LINER	11.70	3600	1800	90	NGC 6172	E +	13.83	8400	9900	80
NGC 3377	E 5-6	11.24	3600	1800	135	NGC 6411	E	12.79	2700	7200	60
NGC 3379	E 1 LINER	10.24	8100	3600	90	NGC 7302	SA (s)0	13.58	4800	6300	100
			3600	1800	70	NGC 7332	S0 pec	12.02	6300	5400	155
NGC 3384	SB 0	10.85	2700	1800	53	NGC 7454	E 4	12.78	3600	2700	148
NGC 3412	SB (s)0	11.45	3600	1800	45	NGC 7585	(R')SA (s)0 pec	12.50	3600	2700	115
NGC 3414	S0 pec	11.96	4800	3600	110	NGC 7619	E	12.10	7200	5400	30
			2700		25	NGC 7626	E pec	12.16	7200	5400	90

Classification and apparent magnitude (B<sub>T</sub>) information from NED (2003).

$$EW_A = \frac{Z}{R} \log \frac{F(\lambda)}{C(\lambda)} d ; \quad (1)$$

$$EW_{\text{mag}} = 2.5 \log \frac{\frac{Z}{R} \frac{F(\lambda)}{C(\lambda)} d}{2} ; \quad (2)$$

where

$$C(\lambda) = F_b \frac{r}{r-b} + F_r \frac{b}{r-b} ; \quad (3)$$

b and r are the mean wavelength in the blue and red pseudocontinuum intervals respectively. We have adopted the

spectral pseudocontinua and bandpasses of the 25 Lick/IDS indices defined in Worthey et al. (1994) and Worthey & Ottaviani (1997).

The conversion between suitable equivalent widths (EW<sub>A</sub>) and magnitude indices is given by

$$\text{Index}^0 = 2.5 \log \frac{1}{Index} \quad (4)$$

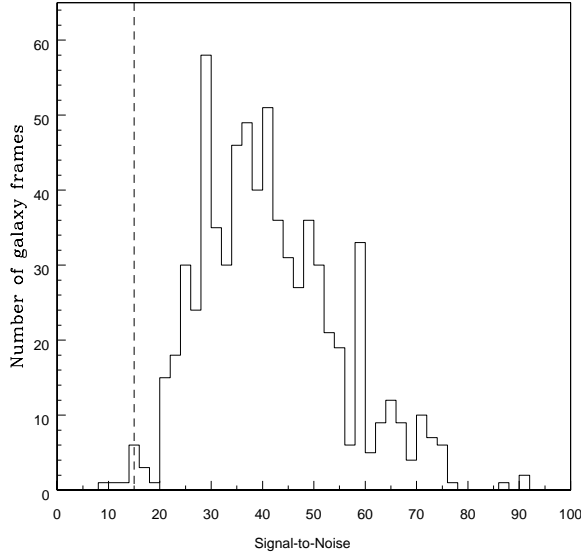
where is the width of the index bandpass.

In this work we will use the index combination MgFe<sup>0</sup> defined in Thomas, Maraston & Bender (2003, TMB03). Note: in their paper this index is called MgFe<sup>0</sup>, but we will

Table 3. Log of observations: stars.

Star	Type	Comment	Star	Type	Comment
H R 0166	K 0V	Lick/ID S std	H R 6770	G 8III	Lick/ID S std
H R 1015	K 3III	Lick/ID S std	H R 6806	K 2V variable	Lick/ID S std
H R 1907	K 0IIIb	Lick/ID S std	H R 6817	K 1III	Lick/ID S std
H R 2429	K 1III variable	Lick/ID S std	H R 6872	K 2III variable	Lick/ID S std
H R 2459	K 5III	Lick/ID S std	H R 7149	K 2III	Lick/ID S std
H R 2574	K 4III	Lick/ID S std	H R 7176	K 1III	Lick/ID S std
H R 2697	K 2III variable	Lick/ID S std	H R 7185	B 5IV	
H R 2854	K 3III	Lick/ID S std	H R 7317	K 4III	Lick/ID S std
H R 2970	G 9III	Lick/ID S std	H R 7480	A 3IV	
H R 3145	K 2III	Lick/ID S std	H R 7576	K 3III	Lick/ID S std
H R 3461	K 0III	Lick/ID S std	H R 7596	A 0III	
H R 3845	K 2.5III variable	Lick/ID S std	H R 7914	G 5V	Lick/ID S std
H R 3905	K 2III	Lick/ID S std	H R 7957	K 0IV	Lick/ID S std
H R 5370	K 3III variable	Lick/ID S std	H R 8165	K 1III	Lick/ID S std
H R 5480	G 7III variable	Lick/ID S std	H R 8430	F 5V	Lick/ID S std
H R 5744	K 2III variable	Lick/ID S std	H R 8665	F 7V	Lick/ID S std
H R 5854	K 2IIIb	Lick/ID S std	H R 8772	F 8V	Lick/ID S std
H R 5888	G 8III	Lick/ID S std	H R 8832	K 3V	Lick/ID S std
H R 5901	K 1IVa	Lick/ID S std	H R 8841	K 0III	Lick/ID S std
H R 5940	K 1IV	Lick/ID S std	H R 8924	K 3III variable	Lick/ID S std
H R 6014	K 1.5IV	Lick/ID S std	H R 8969	F 7V	Lick/ID S std
H R 6018	K 1III-IV variable	Lick/ID S std	BD + 25 4655	?e...	spec. std (Oke 1990)
H R 6136	K 4III	Lick/ID S std	BD + 33 2642	B 2IV p	spec. std (Oke 1990)
H R 6159	K 4III variable	Lick/ID S std	BD + 75 325	O 5p variable	spec. std (Oke 1990)
H R 6299	K 2III variable	Lick/ID S std	Feige 34	D A :	spec. std (Oke 1990)
H R 6458	G 0V variable	Lick/ID S std	G 191-B 2B	D Aw ...	spec. std (Oke 1990)
H R 6710	F 2IV	Lick/ID S std	H z 44	B 2	spec. std (Oke 1990)

Stellar type information from SIMBAD (2003).

Figure 2. Signal-to-noise ratio (per resolution element) for individual frames of our galaxy sample using  $r_e/8$  central extractions. Index measurements were only performed in spectra with  $S/N > 15$  per resolution element (as shown by the dashed line).

adopt simply the notation  $M_{\text{gFe}}$  for their sample definition), and given by equation 5, which should be completely independent of  $\text{Fe}$  variations, according to their models. We also use the index  $\langle \text{Fe} \rangle$  as the average given by equation 6 (dened by Kuntschner 1998):

Table 4. Adopted resolutions to match Lick/ID S.

Wavelength [Å]	FWHM [Å]
3850	4200
4200	4650
4651	5150
5151	5700
5701	6700

$$M_{\text{gFe}} = \frac{p}{M_{\text{gb}} (0.72 F_{\text{e}5270} + 0.28 F_{\text{e}5335})} \quad (5)$$

$$\langle \text{Fe} \rangle = (F_{\text{e}4383} + F_{\text{e}5270} + F_{\text{e}5335})/3 \quad (6)$$

Before measuring the indices, the galaxy spectra were convolved with gaussian curves in order to degrade their resolution to match the Lick/ID S data resolution. We have adopted the average values in the Lick/ID S resolution curve presented in Worthey & Ottaviani (1997). The values we used are summarized in Table 4. We assume that the Lick/ID S resolution continues to degrade to the blue and red end, where we extrapolated the wavelength limits from Worthey & Ottaviani (1997).

#### 4.1 Index errors

A central aspect of this work is that the determination of the errors in all measured and derived parameters is based on the analysis of the distribution of repeated observations.

We consider that the determination of errors through

multiple observation is more reliable than estimates based on photon statistics of object and sky, detector noise, at old errors, etc (e.g., Cardiel et al. 1998). This is because in the repeated observations all main sources of random error are included by default. Furthermore, no assumption about the error distribution function shape is necessary to determine its moments.

Care was taken in order to observe our sample of galaxies repeatedly and whenever possible in different nights or runs. Only galaxies with a minimum of 3 independent observations are included in our sample.

We will consider throughout the paper that the error of the mean ( $\sigma_{\text{mean}}$ , resulting from the repeated measurement of indices in the various galaxy and stellar frames) is:

$$\sigma_{\text{mean}} = \frac{s}{\sqrt{N}} \quad (7)$$

with,

$$s = \sqrt{\frac{1}{N-1} \sum_{i=1}^N (x_i - \langle x \rangle)^2} \quad (8)$$

where  $N$  is the number of frames per galaxy,  $x_i$  is the line-strength measurement in the spectrum  $i$ ,  $\langle x \rangle$  is the mean of the measurements for a galaxy, and  $s$  is the standard deviation.

We must emphasize that all error determinations originated from photon counts, spectral noise, etc, are mere error estimates; the measurement of an error is by definition obtained through repeated experiments. In this work we are presenting data which have the rare advantage of several repeated observations (measurements) per galaxy. On average, to each galaxy we have eight corresponding spectral frames. Therefore, for all the following analysis we will use  $\sigma_{\text{mean}}$  as our error.

Finally, for clarity purposes, all the errors presented in this paper (not only for the indices, but for all other measurements) are 1-sigma errors.

#### 4.2 Emission corrections

Emission lines can be seen in many ellipticals at some level. Spectroscopic surveys of early-type galaxies revealed that about 50–60% of the galaxies show weak optical emission lines (Phillips et al. 1986; Caldwell 1984). The origin of the gaseous component in ellipticals is not yet understood. It could be either of external origin, for example from a cooling flow or from an merger with a small gas rich galaxy; or it could be of internal origin, resulting from stellar mass loss.

The emission-line spectra of giant elliptical galaxies are usually similar to those of LINERs (Low-Ionization Nuclear Emission Regions), where the ionization is provided by an energetic radiation from the nucleus, usually in the form of a power law. However, Filippenko & Terlevich (1992), Binetruy et al. (1994) and Colina & Arribas (1999) showed that post-AGB stars from the old stellar population of an early-type galaxy can also provide sufficient ionizing radiation to account for the observed H $\beta$  luminosity and equivalent width.

More important for this study is that stellar absorption line-strength measurements can be affected if there is emission present in the galaxy, which tells the stellar absorptions. In particular, the Balmer line indices used for age-

dating stellar populations can be severely affected if there is emission, leading to wrong age estimates. González (1993) proposed an empirical emission correction for H $\beta$  using the equivalent width of the emission line [O III] 5007 ( $H\beta = 0.6 \times [\text{O III}] 5007$ , as in Trager et al. 2000a). This turns out to be a very insecure correction because the emission spectra of H $\beta$  regions are strong in H $\beta$  recombination lines, but the strength of [O III] 4959 and [O III] 5007 lines can greatly differ (Osterbrock 1989; Carrasco et al. 1996). We note however, that on average González corrections are shown to be appropriate (Trager et al. 2000a).

Unfortunately, most early-type galaxies that show signs of emission lines are discarded from further spectral analysis in the literature, due to small wavelength coverage of the data (i.e. emission lines important to estimate corrections are not available) or the lack of a reliable emission correction technique. Our OAGH spectra instead, with the availability of the H $\beta$  line information, allow us to use a direct method for emission correction.

In our sample, of the 64 galaxies showing some emission, 29 have a final H $\beta$  correction  $> 0.2 \text{ Å}$ . Twelve galaxies (NGC 2911 and NGC 3941 classified as Seyferts and 10 LINERs) have been corrected using the H $\beta$  emission correction.

Table 5 presents the emission-line index definitions used here for H $\beta$ , [N II] 6584 and [O III] 5007. These definitions work exactly as those of the Lick indices, with a central bandpass flanked by two pseudocontinua.

#### 4.2.1 Balmer lines

Balmer line indices sense mainly the temperature of the turn-off point from the main sequence and thus allow an age estimate of the integrated stellar population (e.g., Buzzoni et al. 1994). Note that the turn-off temperature is also a function of metallicity and therefore the strength of the Balmer absorption is not only a function of age but also a function of metallicity (although to a smaller degree). In reality, the behaviour of Balmer lines at high metallicities seems to be uncertain. For example, Gregg (1994) found, analysing a sample of globular clusters, that the strength of the Balmer lines is only poorly correlated with metallicity above  $[\text{Fe}/\text{H}] = -0.7$ . There are some concerns that stars from other evolutionary phases (e.g., horizontal branch, HB) might contribute significantly to the Balmer absorption. A study of globular clusters by de Freitas Pacheco & Barbuy (1995) showed that blue HB stars may give a substantial contribution to the H $\beta$  absorption (note that the higher order Balmer lines are more strongly affected by HB contribution than H $\beta$ ; e.g., Peterson et al. 2003). Furthermore, they suggest that the HB morphology is correlated with the degree of central concentration in the globular cluster. Whether elliptical galaxies are subject to these effects is not yet known. Maraston & Thomas (2000) have attempted to model the effect of HB morphology by calibrating the Balmer indices with globular cluster sample from Burstein et al. (1984), Covino et al. (1995) and Trager et al. (1998). In Maraston et al. (2003) it can be appreciated a good consistency between Balmer-line indices from models and observations. It is essential, however, to first correct the emission contamination in the Balmer indices before applying model predictions. Widely used in the literature, we are particularly interested in the H $\beta$  index.

Table 5. Emission index definitions.

Index	Central bandpass	Pseudocontinua
[O iii]	5007	4998.000{5015.000 5015.000{5030.000
H		6558.000{6568.000 red = 6620.000
[N ii]	6584	6574.000{6594.000 red = 6620.000

Note: We have assumed that the averaged flux calculated in the blue pseudocontinua for H and [N ii] is equal to the averaged flux in the red continua, because in general the spectra did not have enough wavelength coverage to measure the red pseudocontinua for H and [N ii]. The central wavelength in the red used for the computation of equivalent widths was 6620 Å.

Although the H index is potentially a good age indicator, is the Balmer line more affected by the presence of nebular emission after H, and if not corrected will cause a galaxy to appear older than it really is.

As our wavelength range covers the H line, we have corrected H using EC(H) (which stands for Emission Correction of the H index):

$$EC(H) = \frac{1}{y} \frac{C}{C_{abs}} [EW(H)_{tot} - EW(H)_{abs}] \quad (9)$$

where

$$C = \frac{Cont(H)}{Cont(H)} \quad \text{and} \quad C_{abs} = \frac{Cont(H)}{Cont(H)} : \quad (10)$$

Eq. 9 was derived assuming the following simplified definition for equivalent width:

$$EW(\lambda)_{tot} = 1 - \frac{F(\lambda)_{tot}}{Cont(\lambda)} ; \quad (11)$$

where

$$F(\lambda)_{tot} = F(\lambda)_{em} + F(\lambda)_{abs} \quad (12)$$

and

$$F(H)_{em} = y F(H)_{em} : \quad (13)$$

Cont(H) and Cont(H) are the continua calculated for H and H indices respectively. We assumed  $y = 2.85$  for most galaxies (Osterbrock 1989, Case B of recombination, low density limit at electron temperature of  $10^4$  K). In the equations above, the subscript tot stands for total observed values, em and abs are emission and absorption, respectively. EC(H) is the emission correction in Angstroms for H. We have assumed  $EW(H)_{abs} = 1.03 - 0.08$  Å<sup>y</sup>, derived from  $EW(H)$  measurements in our sample of mainly K stars. Note that the uncertainty in  $EW(H)_{abs}$  takes into account how much a reasonable range of values for  $EW(H)$  in absorption would change the correction.

<sup>y</sup> 0.08 represents the peak to peak range of measurements. Ideally this value should be obtained also from spectral synthesis simulations but there is no simulation yet published with resolution high enough at H to do this estimate.

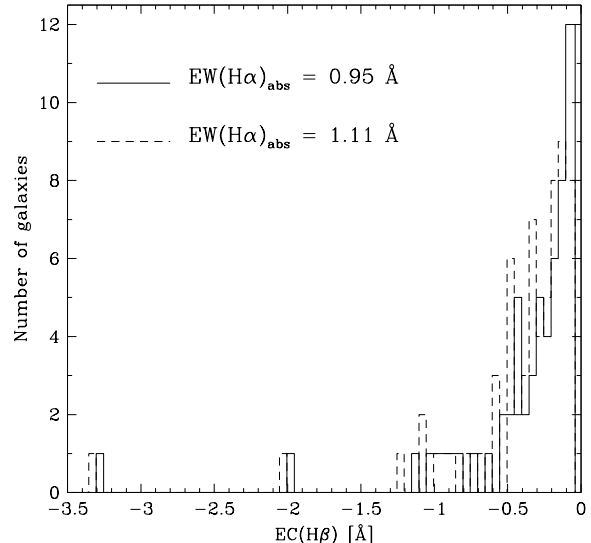


Figure 3. Histogram of emission correction EC(H) assuming two different values for  $EW(H)_{abs}$ . When we take  $EW(H)_{abs} = 0.95$  Å the emission correction is in general less than 0.1 Å smaller than for  $EW(H)_{abs} = 1.11$  Å. The average value for  $EW(H)_{abs}$  used throughout the paper is  $1.03 - 0.08$  Å.

We have corrected the Balmer lines using the term EC(H). The actual correction has been applied to all but 9 galaxies, for which the correction calculated is very small and consistent with zero, and the errors of the correction are larger than the correction itself.

In Figure 3 we show how much the emission correction from eq. 9 would change if we assumed  $EW(H)_{abs} = 0.95$  Å or  $EW(H)_{abs} = 1.11$  Å. The difference in the emission correction for both  $EW(H)_{abs}$  values is generally smaller than 0.1 Å. But this difference is for an extreme variation of  $EW(H)_{abs}$  and must be regarded as an upper limit.

In the expressions above, emission is considered to be negative and absorption positive, therefore  $EC(H)$  should be subtracted from  $EW(H)_{tot}$ . In an attempt to compensate for reddening effects in eq. 9, we have assumed a value of 3.0 for the ratio of intensities  $F(H)_{em}/F(H)_{em}$  of a few dusty galaxies: NGC 2872, NGC 3226, NGC 4125, NGC 4494, NGC 5812, NGC 5813 and NGC 5846 (e.g. Forbes 1991, Tran et al. 2001). The emission correction to H using the H line is presented in column 2 of Table 6.

Trager et al. (2000a) have corrected the H data for emission by subtracting 0.6 [O iii] 5007 emission to the H index. This empirical correction is believed to be valid only in a statistical sense, and not accurate for individual galaxies. For comparative purposes, we have measured the [O iii] index as defined in Kuntschner et al. (2001) and derived the associated emission correction, which is listed in column 3 of Table 6.

Comparing the different emission corrections, the H and the empirical [O iii] 5007 corrections, the difference is small for the majority of galaxies that show emission in the [O iii] 5007 forbidden line (see Figure 4-c). We emphasize that it is very dangerous to rely on the [O iii] 5007 alone because of the uncertainties in the ionization parameter (i.e., one should not assume the same [O iii]/H ratio for

all galaxies). In principle, the H $\alpha$ -based emission correction has less uncertainties than using [O III] 5007. Note that the errors for the [O III] correction in Table 6 are only the propagation of the error from the repeated measurements of the emission line [O III] 5007: further errors are expected since the [O III] 5007/H $\alpha$  ratio may vary greatly from galaxy to galaxy.

Figure 4 shows the difference between the two emission correction methods for H $\alpha$ . Panels (a) and (b) demonstrate the effects of the emission correction in the H $\alpha$  vs MgFe] plane. Panel (c) compares the H $\alpha$  index derived from the [O III] (i.e., H $\alpha$  + EC<sub>[O III]</sub>) and H $\beta$ -based (i.e., H $\beta$  + EC<sub>H $\beta$</sub> ) corrections. The H $\beta$ -based correction (EC<sub>H $\beta$</sub> ) is larger than the [O III] one for most cases, the difference can be up to 1.0 Å.

Panel (d) shows the comparison between our measurements of [O III] and the values in Trager et al. (2000a). The agreement is generally good if we consider the error bars. Note however that we are using an index definition to measure [O III] (Table 5) whereas Trager et al. (2000a, T00a) did not use the same definition. The data analysed in T00a is actually a compilation of the data of Gonzalez (1993), where only the emission profile of the [O III] line was measured.

For the standard elliptical NGC 3379, the H $\alpha$  line index was found to be 1.33 ± 0.09 Å (no emission correction in this value) by Kuntschner (1998), whereas we measure H $\alpha$  = 1.40 ± 0.06 Å (raw value without emission correction). We have measured an emission correction of 0.10 ± 0.08 Å using the H $\alpha$  method, and Kuntschner detected 0.12 Å emission correction for NGC 3379 (using 0.6 [O III] 5007).

The other Balmer-line indices, H $\beta$  and H $\gamma$ , were also corrected using the same procedure as in eq. 9, but assuming  $y = 2.85/0.468 \approx 6.09$  or  $y = 2.85/0.259 \approx 11.00$  for F(H $\beta$ )<sub>em</sub>/F(H $\alpha$ )<sub>em</sub> or F(H $\gamma$ )<sub>em</sub>/F(H $\alpha$ )<sub>em</sub> ratios, respectively (Osterbrock 1989; Case B of recombination, for electron density  $n_e < 10^3$  and  $T_{eff} = 10^4$  K), and changing Cont(H $\beta$ ) for Cont(H $\alpha$ ) or Cont(H $\gamma$ ) accordingly.

The galaxies NGC 1045 and NGC 1453, for which our spectra do not cover the H $\alpha$  line, have been emission corrected for H $\alpha$  using the 0.6 [O III] 5007 approximation. In the same way, H $_{A,F}$  and H $_{A,F}$  for these galaxies have been corrected by the approximated scalings 0.36 [O III] and 0.22 [O III], respectively, adopted in Kuntschner et al. (2002).

#### 4.2.2 Fe5015

Emission can also occur in one of the side-bands of the Lick/IDS indices and raise the continuum which in turn gives larger index values. As pointed out by Kuntschner et al. (2002), the Fe5015 index is affected by [O III] 5007 emission in its central bandpass, and by [O III] 4959 emission in its blue continuum bandpass. These authors have derived a correction to Fe5015 by artificially adding spectral emission and examining the effects on the Fe5015 index. We have used their result, where the index can be corrected by adding +0.61 (±0.01) [O III] 5007 to the Fe5015 measurement. This procedure has large uncertainties and therefore Fe5015 measurements in ellipticals that show emission, either in H $\alpha$  or [O III], should be considered with care.

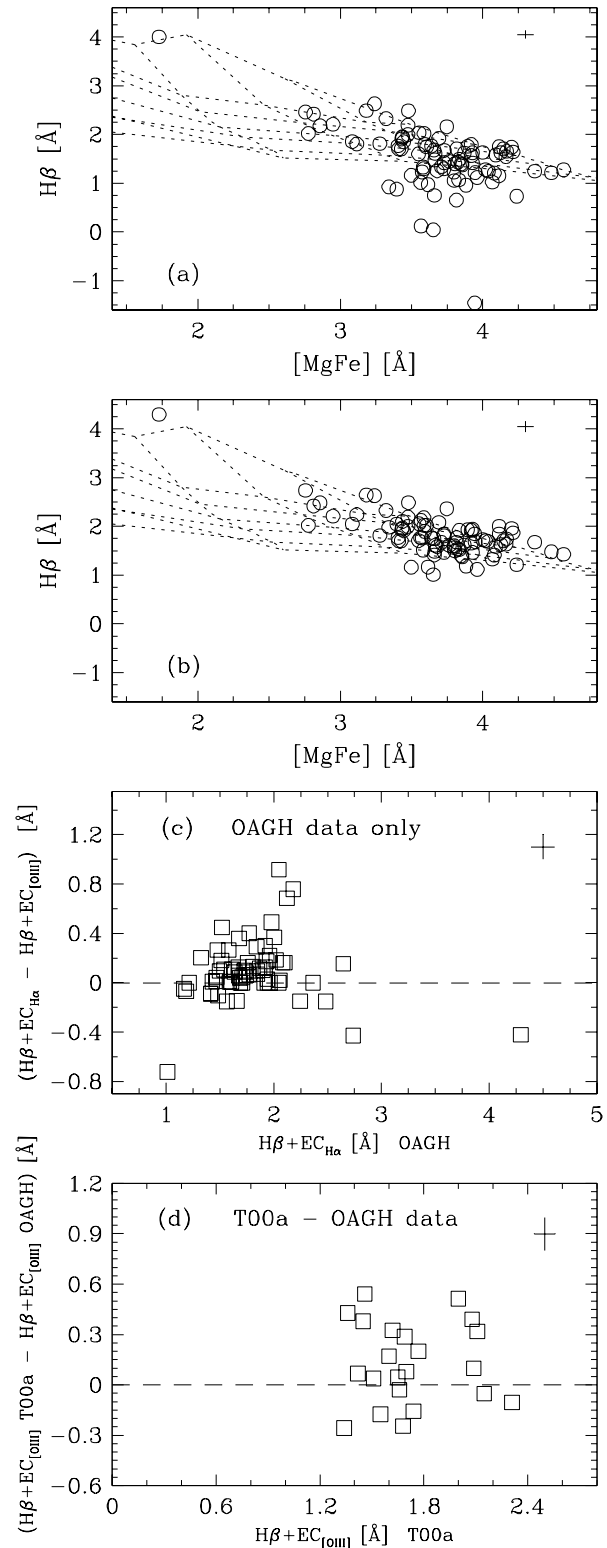


Figure 4. Panels (a) and (b) demonstrate the effect of emission correction in the H $\alpha$  vs MgFe] plane: (a) no correction, (b) EC(H $\alpha$ ) correction applied (Table 6). The dotted lines are single-star population models from Thomas et al. (2003) for a range of ages and metallicities. Panel (c) compares the H $\alpha$  index derived with the [O III] and H $\beta$ -based corrections. Panel (d) presents the comparison between our measurements of [O III] 5007 and the values in Trager et al. (2000a, T00a). The error bars on the top right corner of the plots are averages of the error of the mean.

Table 6. Emission corrections in Angstroms for the galaxies with detected emission lines in the central  $r_e/8$  aperture extractions.

Galaxy (1)	EC (H ) (2)	0.6 (3)	[O iii] 5007 (3)	EW (H ) <sub>tot</sub> (4)	EW ([N ii] 6584) (5)	EC (H A ) (6)	EC (H A ) (7)
NGC 0315	-0.85	0.09	-0.48	0.16	-1.01	0.02	{ -0.71 0.11 -0.50 0.11
NGC 0474	-0.11	0.08	-0.06	0.06	0.77	0.04	{ { { {
NGC 0584	-0.10	0.08	{		0.79	0.01	-0.29 0.02 { { { {
NGC 0720	-0.09	0.08	{		0.82	0.02	{ { { {
NGC 0821	-0.13	0.08	{		0.71	0.05	-0.23 0.08 { { { {
NGC 1045	*		-0.32	0.08	*	*	* *
NGC 1052	-3.30	0.40	-3.23	0.09	-6.89	0.20	-12.22 0.18 -2.75 0.52 -1.95 0.54
NGC 1407	-0.22	0.07	{		0.50	0.03	-0.13 0.01 { { { {
NGC 1453	*		-0.48	0.08	*	*	* *
NGC 1600	-0.23	0.07	-0.11	0.10	0.49	0.04	-0.23 0.10 { { { {
NGC 1700	-0.16	0.08	{		0.64	0.01	-0.52 0.01 { { { {
NGC 1726	-0.33	0.09	-0.21	0.12	0.23	0.15	-0.87 0.15 { { { {
NGC 2128	-1.17	0.12	-0.25	0.10	-1.78	0.05	-3.88 0.03 -0.97 0.16 -0.69 0.16
NGC 2300	-0.07	0.09	{		0.88	0.05	-0.38 0.12 { { { {
NGC 2418	-0.47	0.07	-0.43	0.06	-0.09	0.04	-1.36 0.04 -0.39 0.08 -0.28 0.08
NGC 2513	-0.09	0.09	{		0.82	0.07	{ { { {
NGC 2549	-0.20	0.13	-0.20	0.13	1.26	0.01	{ { { {
NGC 2768	-0.55	0.07	-0.54	0.11	-0.29	0.05	-1.59 0.07 -0.46 0.09 -0.33 0.09
NGC 2872	-0.11	0.09	{		0.77	0.08	-0.16 0.08 { { { {
NGC 2911	-2.00	0.23	-1.32	0.14	-3.77	0.13	-9.55 0.18 -1.66 0.29 -1.18 0.31
NGC 2974	-0.66	0.08	-0.75	0.09	-0.56	0.02	-3.40 0.11 -0.55 0.09 -0.39 0.09
NGC 3091	-0.15	0.08	-0.14	0.08	0.67	0.06	{ { { {
NGC 3098	-0.19	0.11	-0.19	0.11	1.35	0.01	{ { { {
NGC 3115	-0.10	0.08	{		0.80	0.03	{ { { {
NGC 3139	-0.03	0.09	{		0.95	0.05	{ { { {
NGC 3156	-0.29	0.09	-0.71	0.07	0.33	0.13	-0.96 0.02 { { { {
NGC 3193	-0.09	0.08	-0.24	0.01	0.81	0.03	{ { { {
NGC 3226	-0.97	0.10	-1.69	0.05	-1.29	0.02	-2.86 0.13 -0.80 0.13 -0.57 0.13
NGC 3245	-0.75	0.08	-0.35	0.07	-0.78	0.02	-1.64 0.12 -0.63 0.10 -0.45 0.10
NGC 3377	-0.01	0.04	-0.01	0.04	1.37	0.02	{ { { {
NGC 3379	-0.10	0.08	{		0.80	0.03	{ { { {
NGC 3414	-1.02	0.11	-0.96	0.07	-1.42	0.06	-3.42 0.08 -0.85 0.13 -0.60 0.14
NGC 3599	-0.28	0.08	-0.70	0.02	0.37	0.07	-1.60 0.13 { { { {
NGC 3607	-0.43	0.07	-0.13	0.01	0.01	0.01	-2.21 0.02 { { { {
NGC 3608	-0.16	0.08	-0.06	0.08	0.64	0.03	-0.19 0.04 { { { {
NGC 3613	-0.06	0.09	{		0.88	0.06	{ { { {
NGC 3636	-0.06	0.05	-0.06	0.05	1.14	0.11	{ { { {
NGC 3640	-0.02	0.09	{		0.98	0.04	{ { { {
NGC 3665	-0.88	0.09	-0.13	0.01	-1.09	0.02	-1.15 0.05 -0.74 0.11 -0.52 0.12
NGC 3923	-0.13	0.08	{		0.73	0.02	{ { { {
NGC 3941	-0.28	0.07	-0.09	0.11	0.37	0.02	-0.56 0.04 { { { {
NGC 4125	-0.53	0.07	-0.37	0.20	-0.23	0.04	-2.64 0.10 -0.44 0.08 -0.31 0.09
NGC 4261	-0.21	0.08	-0.29	0.05	0.54	0.08	-1.44 0.10 { { { {
NGC 4365	-0.10	0.08	{		0.80	0.02	{ { { {
NGC 4374	-0.55	0.08	-0.25	0.03	-0.28	0.07	-1.63 0.04 -0.45 0.09 -0.32 0.09
NGC 4550	-0.44	0.08	-0.59	0.09	-0.02	0.11	-0.27 0.08 -0.36 0.09 -0.26 0.09
NGC 4754	-0.01	0.09	{		1.01	0.04	{ { { {
NGC 5322	-0.16	0.08	{		0.64	0.02	-0.50 0.02 { { { {
NGC 5353	-0.43	0.07	-0.07	0.06	0.01	0.04	-1.42 0.10 { { { {
NGC 5354	-0.19	0.08	-0.24	0.12	0.57	0.03	-0.14 0.08 { { { {
NGC 5363	-1.05	0.11	-0.56	0.05	-1.50	0.06	-3.12 0.02 -0.88 0.14 -0.62 0.14
NGC 5444	-0.23	0.08	-0.29	0.06	0.49	0.05	-0.42 0.10 { { { {
NGC 5813	-0.33	0.07	-0.06	0.06	0.25	0.05	-0.77 0.14 { { { {
NGC 5831	-0.05	0.09	-0.03	0.10	0.92	0.07	{ { { {
NGC 5845	-0.17	0.08	{		0.61	0.05	-0.31 0.05 { { { {
NGC 5846	-0.45	0.07	{		-0.05	0.03	-1.82 0.08 -0.37 0.08 -0.27 0.08
NGC 5846A	-0.01	0.09	-0.11	0.04	1.02	0.03	{ { { {
NGC 5869	-0.33	0.51	-0.33	0.51	1.14	0.06	{ { { {
NGC 5982	-0.04	0.09	{		0.93	0.01	{ { { {
NGC 6172	-0.30	0.07	-0.46	0.10	0.30	0.04	-1.74 0.08 { { { {
NGC 7302	-0.03	0.09	{		0.96	0.08	-0.29 0.06 { { { {
NGC 7585	-0.16	0.08	{		0.66	0.02	-1.19 0.09 { { { {
NGC 7619	-0.27	0.07	{		0.40	0.03	-0.33 0.05 { { { {
NGC 7626	-0.30	0.07	-0.10	0.07	0.31	0.03	{ { { {

Notes: EC ( ) was derived using  $EW (H )_{abs} = 1.03 \text{ \AA}$  (see eq. 9). The \* symbol is used when H and/or [N ii] fell outside the wavelength limits of the spectra and could not be measured. The | symbol denotes no emission component detected (if EC (H ) shows | it is because no emission was detected in H ). The negative signs denote emission, therefore, the EC ( ) corrections must be subtracted from the effective index measurement, e.g.,  $H_{\text{correct}} = H - EC(H)$ . Columns 4 and 5 are  $EW (H )$  and  $EW ([N ii])$  indices, measured in Angstroms, and defined in Table 5.

## 5 K INEMATICS

Estimates of the galaxy central velocity dispersion  $\sigma_0$  and radial velocity were derived with the IRAF task fxcor. This program uses the cross-correlation method to measure the redshift of the galaxy spectra. A comparison between our redshift determination and that taken from NED is presented in Figure 5-a. Simultaneously, the measured width (FWHM) of the correlation peak is used to estimate the velocity dispersion (FWHM =  $2 \ln 4$ ). The width of the peak will be related to the broadening of the galaxy absorption lines compared to the instrumental resolution of the template star, i.e.,  $\text{FWHM}_{\text{fxcor}}^2 = \text{FWHM}_{\text{galaxy}}^2 + \text{FWHM}_{\text{template}}^2$ .

Within the fxcor task the spectra of galaxy and template are continuum subtracted and cut to a user defined wavelength range (4350–5250 Å] and 5300–6200 Å], for the blue and red observations respectively). Then cross-correlation is performed in the Fourier space, and a "square"

filter is applied to remove large scale variations as well as noise from the spectra. The instrumental dispersion of the OAGH observations is approximately 100 km s<sup>-1</sup> pixel<sup>-1</sup> for the blue region and 80 km s<sup>-1</sup> pixel<sup>-1</sup> for the red region<sup>y</sup>. Multiple measurements of the same galaxy were averaged. We have adopted the error of the mean as our radial velocity dispersion error (equation 7).

We note that the H $\alpha$  feature, present in one of the wavelength intervals, is known to be a source for severe template mismatch for galaxies with strong Balmer absorption (Kuntschner 1998, 2000). Indeed we find some galaxies in our sample with very strong H $\alpha$  feature, i.e., H $\alpha$  > 2.5 Å (NGC 3156 has H $\alpha$  > 3.5 Å). For the same reason, we also have opted to exclude the H $\alpha$  feature from our velocity dispersion measurements. The red wavelength interval on the other hand, encompasses the NaD band, which has an important contribution from interstellar absorption (Dressler 1984). To avoid these template mismatch and contamination problems without losing important information from other wavelengths, we have removed the H $\alpha$  and NaD features from the template spectra used for the cross-correlation. This way, the weight of the H $\alpha$  and NaD regions during the cross-correlation in the Fourier space is kept lower in comparison to any of the other intense correlation features (e.g., the Mg triplet).

Figure 5 presents the comparison between our kinematical measurements and the literature. In panel (a) we see a good agreement (inside the errors) of our radial velocities and values obtained from NED. To do this comparison we have selected in NED the most recent radial velocities derived from optical spectroscopy. In Figure 5-b we show a comparison between our estimated central velocity dispersion and the mean scaled  $\sigma_0$  in the compilation by Prugniel & Simien (1996, PS96). In order to compare our measurements with literature values, we have corrected  $\sigma_0$  to a standard aperture as described by Jørgensen, Franx & Kajrgaard (1995), which scales to a normalized diameter

<sup>y</sup> Note that to measure Lick indices and compare with literature data and models we have to degrade the resolution of the spectra to the values in Table 4. However, to measure velocity dispersion and radial velocity we have used our original observations where no smoothing of the data was performed.

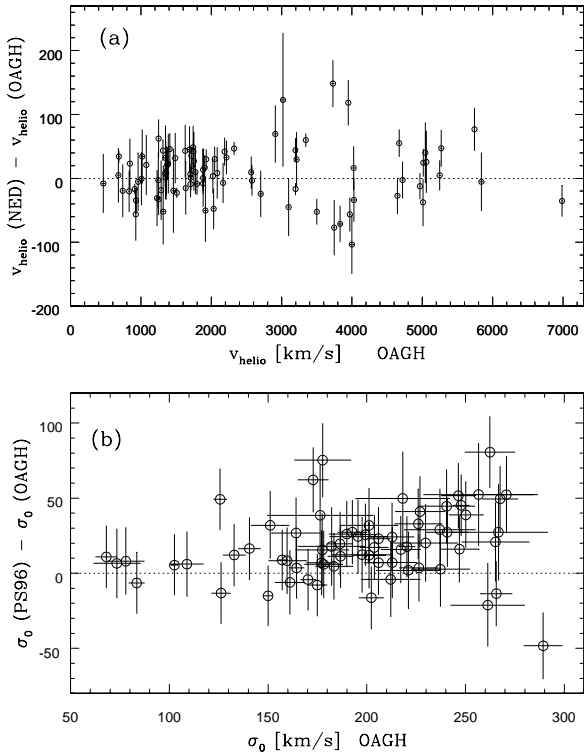


Figure 5. (a) Comparison between our measured radial velocities and published values. (b) Comparison of our measured central velocity dispersions with the  $\sigma_0$  from the compilation of Prugniel & Simien (1996, PS96). The average error bar adopted for the PS96 compilation is 20 km/s.

equivalent to 3.4 arcsec projected on to a galaxy in the Coma cluster. This correction is generally < 10 km/s for our sample. The results agree with those in the literature on a 70% level, using a Kolmogorov-Smirnov test. For galaxies showing  $\sigma_0 < 100$  km/s, systematic errors start to dominate as our spectral resolution is lower than the measurement, and therefore these low velocity dispersions should be considered only as rough estimates. Note that there is a small offset in Figure 5-b, our  $\sigma_0$  is on average 16 km/s smaller than in PS96. For NGC 3379, we obtain  $\sigma_0 = 203 \pm 7$  km/s; Davies et al. (1987) and 201 ± 20 km/s; Franx et al. (1989): 220 ± 3 km/s; Tonry & Davies (1981): 214 ± 15 km/s; Bender et al. (1994): 240 ± 5 km/s; and the average value adopted by Prugniel & Simien (1996) for the compilation of 17 results on NGC 3379 is 221 km/s. We estimate the average uncertainty in the PS96 compilation to be at least of the order of 20 km/s from the multiple measurements, whereas our mean error bar is 11 km/s (or in logarithmic scale, our mean error is 0.024 in  $\sigma_0$ ). Thus, we do not regard as important the offset between our data and the PS96 compilation.

Table 7 lists the adopted radial velocities and aperture re-scaled central velocity dispersions for our galaxy sample.

### 5.1 Velocity dispersion correction to the indices

The observed spectrum of a galaxy is the convolution of the integrated spectrum of its stellar population (s) with the distribution of line-of-sight velocities of the stars and instrumental broadening. These effects broaden the spec-

Table 7. Measured radial velocities ( $v_{\text{helio}}$ ) and central velocity dispersions ( $\sigma$ ) scaled to a standard circular aperture (see text, Section 5).

Galaxy	$v_{\text{helio}}$ [km/s]	$\sigma$ [km/s]	Galaxy	$v_{\text{helio}}$ [km/s]	$\sigma$ [km/s]
ESO 462-G 015	5840	27	NGC 3599	832	9
MCG -01-03-018	5743	10	NGC 3607	960	20
NGC 0016	3100	17	NGC 3608	1229	12
NGC 0221	-123	10	NGC 3610	1704	11
NGC 0315	4968	11	NGC 3613	2034	15
NGC 0474	2325	7	NGC 3636	1741	13
NGC 0584	1883	11	NGC 3640	1251	12
NGC 0720	1725	9	NGC 3665	2049	10
NGC 0750	5248	16	NGC 3923	1796	13
NGC 0751	5270	15	NGC 3941	926	9
NGC 0777	5015	8	NGC 4125	1347	35
NGC 0821	1717	11	NGC 4261	2191	11
NGC 0890	4027	26	NGC 4365	1248	14
NGC 1045	4646	9	NGC 4374	1007	14
NGC 1052	1510	6	NGC 4494	1344	11
NGC 1132	6988	17	NGC 4550	465	21
NGC 1407	1774	19	NGC 4754	1347	9
NGC 1453	3999	28	NGC 5322	1754	16
NGC 1600	4720	17	NGC 5353	2169	16
NGC 1700	3971	13	NGC 5354	2579	13
NGC 1726	4025	24	NGC 5363	1077	9
NGC 2128	3019	30	NGC 5444	3948	10
NGC 2300	1905	7	NGC 5557	3213	18
NGC 2418	5043	7	NGC 5576	1487	6
NGC 2513	4672	13	NGC 5638	1637	11
NGC 2549	1019	14	NGC 5812	1885	13
NGC 2768	1360	6	NGC 5813	1929	7
NGC 2872	3196	11	NGC 5831	1629	8
NGC 2911	3199	7	NGC 5845	1410	22
NGC 2974	1916	23	NGC 5846	1708	17
NGC 3091	3729	17	NGC 5846A	2217	16
NGC 3098	1387	13	NGC 5854	1691	35
NGC 3115	685	7	NGC 5864	1885	4
NGC 3139	1412	10	NGC 5869	2085	4
NGC 3156	1318	16	NGC 5982	2911	22
NGC 3193	1377	18	NGC 6172	5009	8
NGC 3226	1287	11	NGC 6411	3747	16
NGC 3245	1314	6	NGC 7302	2703	16
NGC 3377	679	17	NGC 7332	1250	16
NGC 3379	912	6	NGC 7454	2022	5
NGC 3384	740	15	NGC 7585	3499	14
NGC 3412	844	10	NGC 7619	3833	27
NGC 3414	1460	23	NGC 7626	3345	9

tral features, in general reducing the observed line-strength compared to intrinsic values. In fact, it is well known that there is a velocity dispersion dependence on the indices and it needs to be corrected (e.g., Gonzalez 1993; Jørgensen et al. 1995). In order to compare the raw index measurements in galaxies with the model predictions we calibrate the indices to zero velocity dispersion. The procedure adopted here is to broaden the spectra of template stars with gaussians of  $\sigma = 20\text{--}400$  km/s in bins of 20 km/s. The indices are then measured for each bin and a correction factor is determined. The correction factor has the form  $C(\sigma) = \text{index}(\sigma=0)/\text{index}(\sigma)$  for indices measured in Ångström s, and  $C(\sigma) = \text{index}(\sigma=0)/\{\text{index}(\sigma)\}$  for indices given in magnitudes. It is important to stress that derived correction factors are only useful if the stars used for the simulations resemble the galaxy spectra. For this reason, we have opted to

build a composite stellar spectrum template, and compared the resulting super-template with the spectra of NGC 3379, observed in every run. The super-template was created by averaging different stellar-type spectra selected from Table 3, carefully allocating more weight to the K giant stars. Figure 6 shows the dependence of the correction factor on for 25 Lick indices measured in stars; the dotted bars denote the uncertainty range in the correction due to errors in the index measurements. A polynomial fitting to the curves in Figure 6 allowed for the velocity dispersion corrections, which were then added or multiplied (if in units of mag or Å respectively) to the raw index measurements of the resolution corrected galaxy spectra. In this procedure, the errors in  $\sigma$  are then propagated to the index errors.

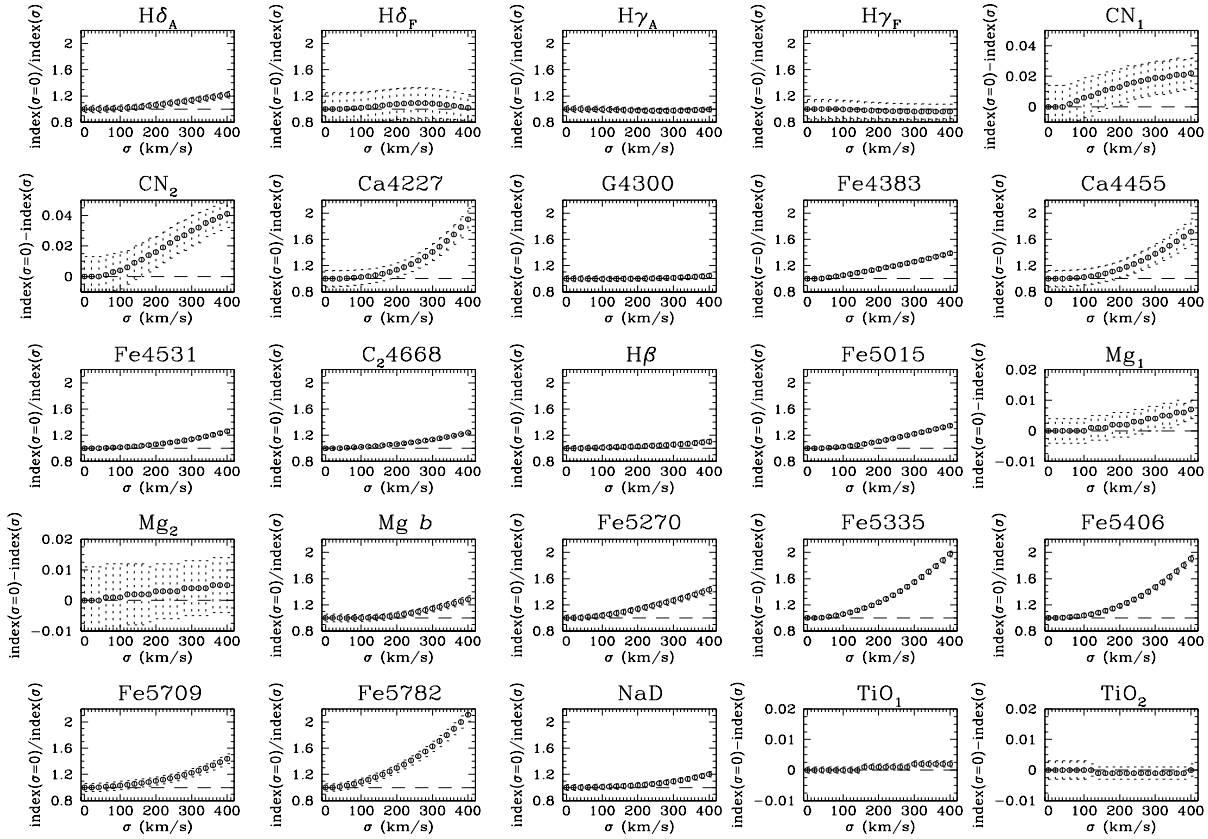


Figure 6. Velocity dispersion corrections. The broadening and index measurements were performed on a composite stellar spectrum template that very well matches the spectra of the bona fide elliptical galaxy NGC 3379. The dotted bars represent the uncertainties derived from the index measurement errors. The dashed line is used as a visual guide-line for no correction applied.

## 6 FINALLY CENTRAL ABSORPTION LINE STRENGTH

To remove any remaining systematic offset between our measurement and the Lick/IDS, we have compared them measurements of 25 line-strength indices of our 45 stars observed in common with Lick. Generally there is good agreement between the two data sets, and only small offsets are found (see Figure 7, for an offset-corrected comparison). The mean offsets and associated errors for each index are summarized in Table 8. These offsets were then applied to our data.

The final corrected central  $r_e/8$  index measurements and associated errors for our galaxy sample are presented in the Appendix B in Table B 1.

### 6.1 Summary: the sample and Lick indices

Trager et al. (1998) have demonstrated that index errors can masquerade as real trends in the determination of ages, metallicities and their correlations with velocity dispersion. Here we give special treatment to the  $H_{\alpha}$ -index because this index will be used in subsequent papers to infer ages and metallicities, using for example,  $H_{\alpha}$ -Mg[Fe] index diagram s. It happens so that the information on  $H_{\alpha}$  errors is commonly used to separate and select the best galaxy data in the literature. The sample used by Trager et al. (1998) had a typical error of  $H_{\alpha} = 0.191 \text{ \AA}$ . A reasonable guide is that  $H_{\alpha}$  must

Table 8. Lick/IDS sets.

Index	O set (Lick/IDS)	OAGH
$H_{\alpha}$	0.07	0.18 \AA
$H_{\beta}$	0.09	0.09 \AA
$H_{\gamma}$	+ 0.16	0.10 \AA
$H_{\delta}$	+ 0.18	0.05 \AA
$CN_1$	0.000	0.005 mag
$CN_2$	0.011	0.006 mag
$Ca4227$	0.04	0.04 \AA
$G4300$	0.03	0.08 \AA
$Fe4383$	+ 0.19	0.09 \AA
$Ca4455$	+ 0.29	0.05 \AA
$Fe4531$	+ 0.27	0.08 \AA
$C_24668$	+ 0.06	0.10 \AA
$H$	0.06	0.04 \AA
$Fe5015$	0.17	0.08 \AA
$Mg_1$	+ 0.011	0.002 mag
$Mg_2$	+ 0.023	0.003 mag
$Mg_b$	0.09	0.05 \AA
$Fe5270$	0.07	0.04 \AA
$Fe5335$	0.12	0.05 \AA
$Fe5406$	0.03	0.03 \AA
$Fe5709$	+ 0.05	0.03 \AA
$Fe5782$	+ 0.05	0.02 \AA
$NaD$	+ 0.09	0.03 \AA
$TiO_1$	+ 0.006	0.001 mag
$TiO_2$	+ 0.002	0.002 mag

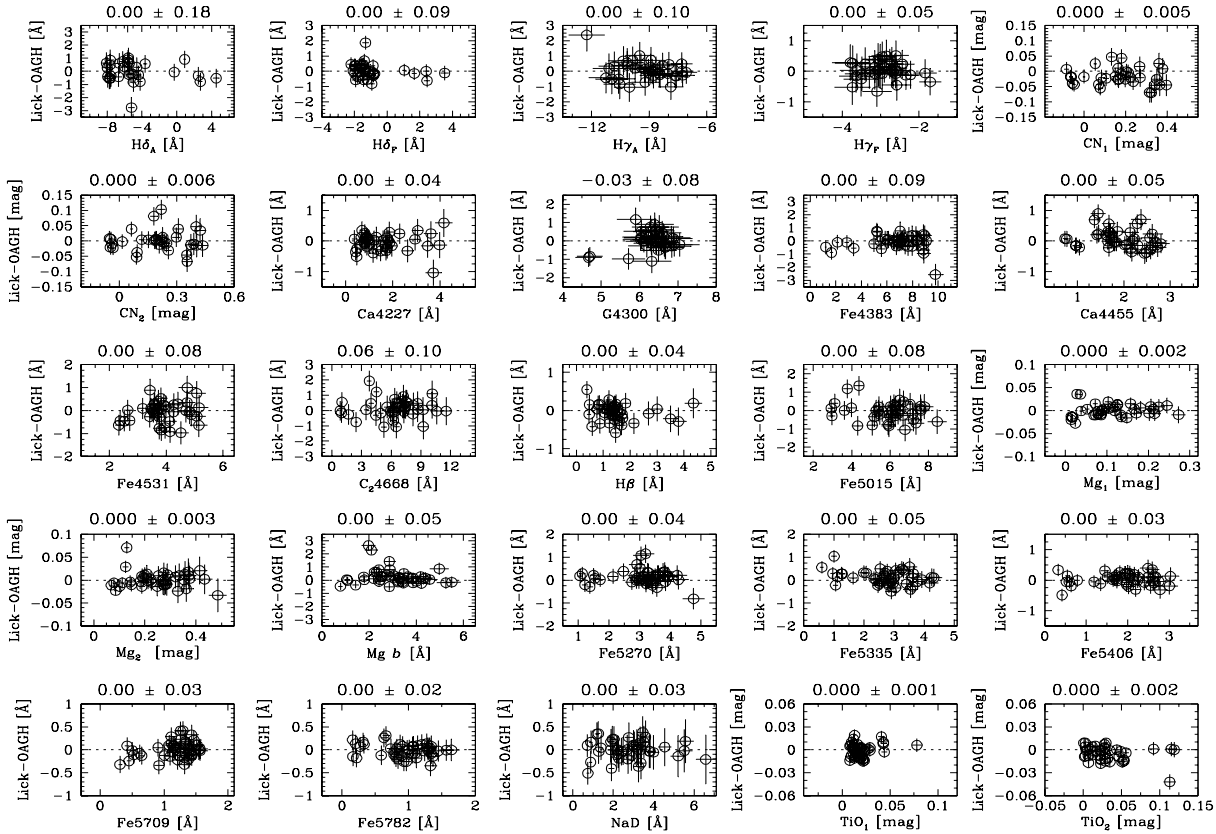


Figure 7. Comparison between our line-strength measurements and Worthey et al. (1994) for 45 stars in common. Our data were corrected for the Lick/IDS set prior to comparison. The remaining offset and associated 1-sigma error are shown above each subplot. The offsets are summarized in Table 8.

be accurate to 0.1 Å in order to determine reliable ages and metallicities.

Figure 8 shows a histogram of  $H\beta$ -index errors. These errors take into account the errors in the emission correction, i.e., we have propagated the errors of the emission correction into the new  $H\beta$  correct error following eq. 9. The median error of the sample is 0.125 Å. Previous to the emission correction, the median error of our data was 0.086 Å.

The errors in the determination of ages and metallicities from index-index diagram will be addressed again in a subsequent paper.

Our survey has the advantage of covering a large wavelength range, from 3850 Å to 6700 Å, giving  $H\beta$  information which is important for emission correction. Of the 86 galaxies with  $S/N > 15$  (for  $r_e/8$  aperture, and per resolution element), 52 had  $H\beta$ -index corrected for emission, the corrections varied from as small as 0.1 Å to as large as 3.3 Å for NGC 1052; 41 galaxies present [O III] 5007 emission, of which 16 also show obvious  $H\beta$  emission. Most of the galaxies in the sample do not show obvious signs of disturbances nor tidal features in their morphologies, although 11 galaxies belong to the Arp catalogue of peculiar galaxies (Arp 1966), of which only three (NGC 750, NGC 751 and NGC 3226) seem to be strongly interacting.

We have applied a better method for emission correction of the Balmer-line indices than the use of the uncertain 0.6 [O III] estimation. The new correction uses the intensity and equivalent width of the  $H\beta$  index (defined in Table 5).

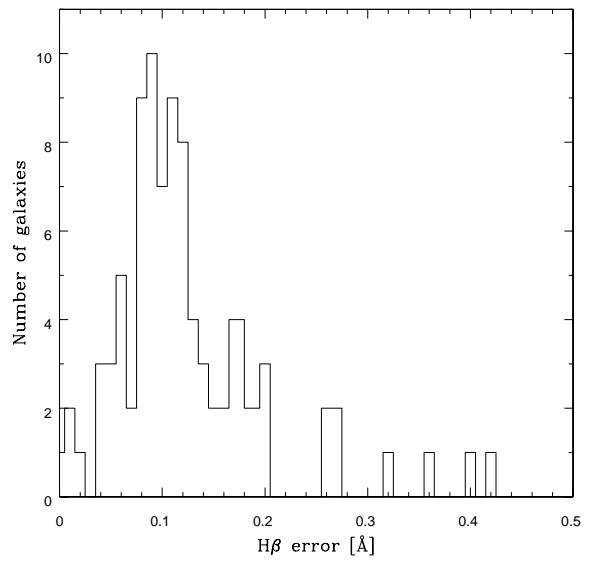


Figure 8. Histogram of  $H\beta$ -index errors (error of the mean per galaxy). These uncertainties take into account the errors in the emission correction. The median error of the sample is 0.125 Å.

We note that nebular emission could still be affecting the ages and metallicities derived from most of the data in the literature.

## 7 INDEX { RELATIONS

In this Section, we will compare  $\log_{10}$  with indices measured in magnitudes. Indices originally measured in Angstroms are converted to magnitudes as explained in eq. 4, and now denoted with a prime, i.e.,  $H'$  in magnitudes will be called  $H^0$ .

The dynamical properties of galaxy cores are closely connected with their stellar populations, implied by the relatively small scatter in the colour- $\log_{10}$ ,  $Mg_2^0$ -relations found in previous investigations (e.g. Terlevich et al. 1981, Burstein et al. 1988, Bower, Lucey & Ellis 1992). The prominence of the  $Mg_2^0$  relation suggests that other metal line-strength indices should also exhibit a correlation with the central velocity dispersion. We present in Figures 9 and 10 the index- $\log_{10}$  relations for  $\langle Fe \rangle^0$ ,  $CN_1$ , two Balmer-line indices ( $H^0$ ,  $H_A^0$ ),  $Mgb^0$  and  $Mg_2^0$ .

We have performed ordinary least square fits with  $Y = \text{Index}^0$ , as the dependent variable (hereafter the  $(Y|X)$ ) fit; solid line in Figures 9 and 10) and also a fit in which  $\text{Index}^0$  is the independent variable (dotted line in Figures 9 and 10). Isobe et al. (1990) recommend the  $(Y|X)$  fit for scientific problems where one variable is clearly an effect and the other the cause. The combination of the regressions of  $Y$  on  $X$  and  $X$  on  $Y$  allows us to compute the linear correlation coefficient  $R = \frac{\sum b_i}{\sqrt{\sum b_i^2}}$ , where  $Y = a + bX$  and  $X = a^0 + b^0Y$ . Here both regressions are shown to illustrate how different fitting methods lead to different results. For the  $\text{Index}^0$ - $\log_{10}$  relation analysis, we favour the  $(Y|X)$  method for two reasons: (1) consistency with previous authors, as frequently they fit their data using the  $(Y|X)$  method; (2) at least the Mg content of a galaxy seems to be driven by the central potential of the galaxy (see conclusions of Colless et al. 1999) which is approximated by its central velocity dispersion  $\sigma_0$ . The code used to derive the  $(Y|X)$  fits is an IRAF implementation of the Fortran code by Bevington (1969). Table 9 presents the  $(Y|X)$  fit values and uncertainties for all the sample (E+S0s).

In Figures 9 and 10 we compare our results with the Fornax cluster sample from Kuntschner (2000; 22 galaxies), and the 'mixed' galaxy sample from Kuntschner et al. (2001; 72 galaxies), which includes Virgo and Coma clusters galaxies, a few S0s and galaxies in less dense environments. Consistent with the results of Kuntschner (2000) and Kuntschner et al. (2001, 2002), we find a weak correlation between the  $\langle Fe \rangle^0$  index and  $\log_{10}$ . The slope of the  $\langle Fe \rangle^0$ - $\log_{10}$  relation is the steepest in Table 9. The  $Mg_2^0$ - $\log_{10}$  and  $\langle Fe \rangle^0$ - $\log_{10}$  relations presented here for group, field and isolated galaxies are not significantly different from those of cluster E/S0s (see fits plotted in Figures 9 and 10). Nonetheless, the slopes of the other relations (except  $CN_1$ - $\log_{10}$ , which has no comparison) are significantly different with respect to previous authors, even though all relations are still following the trend of increasing metallicity with increasing velocity dispersion.

It is necessary to point out that the shift in the dashed lines between the fit of  $\langle Fe \rangle^0$  and  $Mgb^0$  indices for K 2000 and K 2001 in Figures 9(b) and 9(c) is probably related to the fact that, while K 2000 are 'central' values for the equidistant Fornax cluster galaxies, K 2001 values are for a fixed linear aperture as in this paper. We have no explanation for the shift in  $\langle Fe \rangle^0$  indices between K 2001 and this work,

Table 10. Kuntschner et al. (2000, 2001) least square fit results.

K 2000:						
$Mg_2^0$	=	(0.127	0.054)	+	(0.191	0.023) $\log_{10}$
$Mgb^0$	=	(0.056	0.044)	+	(0.102	0.020) $\log_{10}$
$\langle Fe \rangle^0$	=	+ (0.015	0.053)	+	(0.038	0.023) $\log_{10}$
$H^0$	=	+ (0.106	0.015)	(0.020	0.007) $\log_{10}$	
$H_A^0$	=	(0.038	0.044)	(0.045	0.019) $\log_{10}$	

K 2001:						
$Mgb^0$	=	(0.163	0.031)	+	(0.142	0.013) $\log_{10}$
$\langle Fe \rangle^0$	=	(0.034	0.015)	+	(0.021	0.006) $\log_{10}$

other than that K 2001 includes a more 'mixed' sample of galaxies.

The fit values for the Fornax cluster in Kuntschner (2000) and for the field, group and cluster galaxies in Kuntschner et al. (2001) are shown in Table 10.

Figures 9-d and 10-a show the index- $\log_{10}$  relations for two Balmer-line indices ( $H^0$  and  $H_A^0$ ). Both indices show negative correlations with the central velocity dispersion. In Figure 10-b, the  $CN_1$  index correlates with  $\log_{10}$  almost as strongly as  $Mg_2^0$ , however with larger scatter. In a subsequent paper we will discuss the sensitivity of CN indices to elements like Mg.

Note that on average most S0 galaxies have slightly lower  $\log_{10}$  values than the bulk of Es. Remarkably, bulges of S0s follow the same general relation with  $\log_{10}$  as the elliptical galaxies. Yet, the peculiar S0 galaxy NGC 3156 shows a Mg absorption which is too low by 0.080 and 0.040 mag for  $Mg_2^0$  and  $\langle Fe \rangle^0$  respectively. As we will in a subsequent paper, this galaxy has a very young (luminosity weighted) central stellar population for an early-type galaxy of its brightness and velocity dispersion. This may be an extreme case, but it demonstrates nicely how the Mg, Fe, H,  $H_A^0$  relations can be influenced by young stellar populations in the centre of the galaxy. We also note that the bulk of galaxies in our sample with higher  $H^0$  and  $H_A^0$  index values (i.e., indicative of younger stellar populations according to single-star population models [forthcoming paper]) have relatively small velocity dispersions. We note also that of the four galaxies with  $\log_{10} < 2.0$  in our sample, two are classified as field galaxies (NGC 3599, NGC 4550), and the other two are NGC 221, a compact dwarf elliptical, and NGC 3156, an outlier galaxy in our sample (c.f., Figures 9 and 10).

On average our Mg-absorption strength is lower than in the Fornax galaxies from Kuntschner (2000). This could either be a metallicity or/and age related effect. As we have seen, there is a general trend that the presence of young stellar populations moves galaxies to lower Mg values. Some examples of anomalously low Mg-absorption values were previously identified by Jørgensen (1997). In agreement with this trend, we can also argue that our  $H^0$  values are slightly higher (i.e., younger) than the cluster sample. This may be one indication that on average our OAGH sample is relatively younger in comparison to the mean age of galaxies in Fornax.

The bottom panels in Figures 9 and 10 show the residuals from the Index- $\log_{10}$  fits ( $Y|X$ ). The dashed lines indicate the 1- $\sigma$  intrinsic scatter; that is  $+0.016$  and  $+0.004$  mag for  $Mgb^0$  and  $\langle Fe \rangle^0$  respectively. We have estimated the intrinsic scatter by requiring

Table 9. Least square t results.

Index		< Index <sup>0</sup> > [mag]	< Index <sup>0</sup> > [mag]	< Δ > [mag]	R <sup>y</sup>
M g <sub>2</sub>	= 0.198 ( 0.048) + 0.218 ( 0.021)	log <sub>10</sub>	0.024	0.003	0.023 0.75
M gb <sup>0</sup>	= 0.277 ( 0.012) + 0.190 ( 0.005)	log <sub>10</sub>	0.016	0.004	0.016 0.74
< Fe> <sup>0</sup>	= 0.003 ( 0.014) + 0.044 ( 0.006)	log <sub>10</sub>	0.007	0.005	0.004 0.61
C N <sub>1</sub>	= 0.457 ( 0.069) + 0.244 ( 0.030)	log <sub>10</sub>	0.036	0.006	0.035 0.61
H <sub>0</sub>	= 0.267 ( 0.028) 0.086 ( 0.012)	log <sub>10</sub>	0.012	0.003	0.011 0.55
H <sub>A</sub> <sup>0</sup>	= 0.110 ( 0.033) 0.108 ( 0.015)	log <sub>10</sub>	0.016	0.004	0.015 0.63

y R is the linear correlation coefficient calculated as  $R = \frac{P}{\sqrt{bb^0}}$ , where

$\log_{10} = a + b \text{Index}^0$ , and  $\text{Index}^0 = a^0 + b^0 \log_{10}$ . The correlation R varies from 0 to 1.

< Index<sup>0</sup> > : Average deviation from t (excluding NGC 3156).

< Index<sup>0</sup> > : Average individual error in the index.

< Δ > : Estimated intrinsic scatter (excluding NGC 3156).

Table 11. Correlation matrix of the residuals ( ) of the log<sub>10</sub>-Index relations.

M g <sub>2</sub> [mag]	M gb <sup>0</sup> [mag]	< Fe> <sup>0</sup> [mag]	C N <sub>1</sub> [mag]	H <sub>0</sub> [mag]	H <sub>A</sub> <sup>0</sup> [mag]
M <sub>B</sub> [mag]	0.17	0.40	0.11	0.17	0.02
log <sub>10</sub> [mag]	0.08	0.27	0.19	0.03	0.08
M g <sub>2</sub> [mag]	0.66	0.24	0.48	0.46	0.39
M gb <sup>0</sup> [mag]	0.57	0.38	0.46	0.39	0.42
< Fe> <sup>0</sup> [mag]	0.45	0.17	0.84	0.32	0.43
C N <sub>1</sub> [mag]	0.59	0.26	0.40	0.71	0.31
H <sub>0</sub> [mag]	0.47	0.21	0.47	0.30	0.82
H <sub>A</sub> <sup>0</sup> [mag]	0.51	0.22	0.67	0.32	0.62

Note: Linear correlation coefficients (R) calculated as  $R = \frac{P}{\sqrt{bb^0}}$ , where

$\log_{10} = a + b \text{Index}^0$ , and  $\text{Index}^0 = a^0 + b^0 \log_{10}$ .

The correlation R varies from 0 to 1.

$$\frac{\sum_{k=1}^N \text{Index}_k^{02}}{\sum_{k=1}^N \text{Index}_k^{02} + i^2} = 1 \quad (14)$$

where  $\text{Index}_k^{02}$  is the deviation from the fitting relation for each galaxy,  $\text{Index}_k^0$  are the individual errors in  $\text{Index}^0$ , and  $i$  is the estimated intrinsic scatter. The values for the intrinsic scatter are shown in the last column of Table 9. Comparing with previous results, Colless et al. (1999) analysed 736 early-type galaxies from their EFA R cluster galaxy sample with an intrinsic scatter for M gb<sup>0</sup> of 0.016 mag. Kuntschner et al. (2001), for a sample of 72 early-type galaxies from different environmental regions, derived an intrinsic scatter of 0.012 mag in M gb<sup>0</sup>, smaller than ours by 0.004 mag.

In Figure 9-a, the M g<sub>2</sub>-<sub>0</sub> relation, we also show the least square bisector t by Guzman et al. (1992) from a sample of 51 Coma cluster ellipticals. The Coma cluster is the densest cluster in the local universe (at average distance

7000 km/s). The bisector t by Guzman et al. (1992) is

$$M g_2 = (0.316 \pm 0.003) + 0.260 \log_{10} \quad (15)$$

The observed scatter for their M g<sub>2</sub>-<sub>0</sub> relation is 0.020 mag. The intrinsic scatter is 0.016 ± 0.002 mag. Guzman et al.'s t is very similar to the results of Colless et al. (1999) for the EFA R sample of cluster galaxies. Colless et al. (1999) maximum likelihood t for M g<sub>2</sub>-<sub>0</sub> relation of 423 cluster early-type galaxies is  $M g_2 = -(0.305 \pm 0.064) + (0.257 \pm 0.027) \log_{10}$ .

Note that the slope of our t for the M g<sub>2</sub>-<sub>0</sub> relation is

similar to the slopes of the EFA R and Coma cluster samples. However, comparing only the slopes and scatter of the relations is not telling us about important differences between the samples: we would need to analyse the distribution of the galaxies in the M g<sub>2</sub>-<sub>0</sub> relations to infer further conclusions about the different environment (cluster, field). Indeed, most of the galaxies in the EFA R sample are clustered around  $\log_{10} = 2.35$ -2.40, and go beyond  $\log_{10} = 2.5$ , which is a slightly different range of values from that covered by our group, field and isolated galaxies. We can do a better comparison with the Coma cluster sample of Guzman et al. (1992) as they list the velocity dispersions and M g<sub>2</sub> index strength for their sample. The average  $\log_{10}$  in Guzman et al.'s sample is 2.32 (error of the mean: 0.02, for a sample of 51 galaxies), whereas in our sample the average value is  $\log_{10} = 2.302$  (error of the mean: 0.014, for a sample of 86 galaxies). The average M g<sub>2</sub> index strength in the Coma cluster sample is 0.282 (error of the mean: 0.004) and in our sample is 0.307 (error of the mean: 0.004). Thus, the distribution of galaxies in the M g<sub>2</sub>-<sub>0</sub> relation for high or less dense regions is very similar. We learn from these comparisons that, perhaps surprisingly, cluster, group and field galaxies have very similar M g<sub>2</sub>-<sub>0</sub> relations, and environment does not seem to be a key parameter here. It is relevant to note here that Bernardi et al. (1998) also found, for a large sample of 931 early-type galaxies, that objects assigned to cluster, group or field follow almost identical M g<sub>2</sub>-<sub>0</sub> relations.

We note that age and metallicity may conspire to keep

the relation tight (Trager et al. 2000b) and hence its usefulness as a probe of different galactic environments may be limited.

What causes the spread in the Index $^{0-0}$  relations?

Two obvious potential sources of scatter are age and metallicity. In the case of the M g- $0$  relation, it has been investigated by many authors, but perhaps the best paper on this topic is by Bender et al. (1993). They conclude that if the spread in the M g- $0$  relation at a given  $z$  is due to age only then the mass spread in age is only 15% for bright dynamically hot galaxies. Alternatively, if the spread is only due to metallicity then they infer a mass spread of about 15% in metallicity. A similar analysis by Colless et al. (1999) using up-to-date model predictions and constraints from the Fundamental Plane and slightly larger numbers.

With the help of stellar population models one can translate the intrinsic spread in M g $^0$  for example, at a given  $z$ , into age and metallicity spreads. To simplify this exercise, we assume initially that there are no other sources of scatter, and that age and metallicity are not correlated, or only mildly so (see Colless et al. 1999 for more detailed analysis). Using Colless et al. (1999) calibration of M g $^0$  as a function of log age and metallicity, we find for our data set at a given  $z$  and at fixed metallicity a spread of  $\Delta t/t = 67$  per cent in age and at fixed age a spread of  $\Delta Z/Z = 43$  per cent respectively. Kuntschner et al. (2001) found 49 and 32 per cent respectively.

In Table 11 we investigate the effects that age (in the form of the Balmer-line indices, H $_4$ , H $_3$ , for example), metallicity (using M g, Fe, as metallicity indicators), absolute magnitude ( $M_B$ ), and  $z$  may have on the scatter of the Index- $0$  relations. Table 11 presents the results of the linear correlations coefficients ( $R$ ) from the residuals ( $\epsilon$ ) vs  $M_B$ , log  $z$ , M g, Fe, H $_4$ , H $_3$  and CN indices.

In general the residuals of the Index- $0$  relations better correlate with the strength of the Index itself, i.e., M g $_2$  shows  $R = 0.66$  for a correlation with M g $_2$ , H $_4^0$  shows  $R = 0.82$  for a correlation with H $_4^0$ , and so on. For the M g $2-0$ , the scatter of the relation grows with decreasing M g $_2$  strength. In the case of H $_4^0$ , the scatter grows with increasing H $_4$  strength. Note however that our sample, like most of the currently available samples, is not complete and is still lacking low-luminosity and low- $z$  galaxies. Another work by Concannon, Rose & Caldwell (2000) indicates that the spread in age at a given  $z$  increases towards the low velocity dispersion range. Hence incompleteness at low velocity dispersions is potentially a source for bias. Finally, the correlation of the residuals with H $_4$  index is not specifically significant to clearly associate the intrinsic scatters in our sample with possible age variations. The same weak correlations are observed for metal-line indices vs scatter, for our sample.

There may well be other effects responsible for the scatter, such as variations in the M g-overabundance at a given  $z$ . We leave further discussion to a forthcoming paper where we investigate the relations of  $\epsilon$  with age, metallicity and /Fe ratios and the scatter of the M g- $0$  relation with age and metallicity.

Finally, we would like to comment on the work of Worthey and Collobert (2003), using a compilation of nearly 2000 M g- relations from the literature to assess the ques-

tion of the importance of mergers in the formation of early-type galaxies. Their simulations suggest that the evolution of median M g index strength is not a good discriminator between mergers and passive evolution and that better discriminator such as M g- scatter and asymmetry require samples of more than 1000 objects with accuracies similar to today's local measurements to really establish further constraints in the formation scenario of early-type galaxies.

## 8 SUMMARY

We have argued that there is a sparsity of field and group galaxies in stellar population studies. Many predictions of the hierarchical clustering models compare the properties of field, cluster and group galaxies, however most of the field and group galaxy data available to date tend to be of lower quality than the cluster data. We hope that this work and its high quality data will serve as a step to improve the present state of knowledge based on early-type galaxies from low-density environments.

We carried out an observationally homogeneous survey of 86 local early-type galaxies of mainly group (65), field (10) and isolated (8) objects with the aim of determining nuclear parameters, kinematic (this paper), age and metallicity gradients (subsequent paper).

It is important to emphasize that our survey has the advantage of covering a large wavelength range, from 3850 Å to 6700 Å, giving H $_4$  information which is important for emission correction (Section 4.2).

Most of the galaxies in the sample do not show obvious signs of disturbances nor tidal features in their morphologies, although 11 galaxies belong to the Arp catalogue of peculiar galaxies (Arp 1966), of which only three (NGC 750, NGC 751 and NGC 3226) seem to be strongly interacting. Of the 86 galaxies with S/N > 15 (per resolution element, for r<sub>e</sub>/8 aperture), 57 had H $_4$ -index corrected for emission, the average correction was +0.190Å in H $_4$ ; 42 galaxies have [O iii] 5007 emission correction, of which only 16 also show H $_4$  emission.

Our data allowed us to apply a better method for emission correction of the Balmer-line indices than the use of the uncertain 0.6 [O iii] estimation. The new correction uses the intensity and equivalent width of the H $_4$  index (defined in Table 6). We note that nebular emission could still be affecting the ages and metallicities derived from most of the data in the literature.

A central aspect of this work is that the determination of the errors in all of the measured and derived parameters is based on the analysis of the distribution of repeated observations. In this paper we are presenting data which have the advantage of several repeated observations (measurements) per galaxy. On average, to each galaxy we have eight corresponding spectral frames.

Our main findings are that the index- $0$  relations presented for low-density regions are not significantly different from those of cluster E/S0s. The slope of the index- $0$  relations shown in Section 7 does not seem to change for early-type galaxies of different environmental densities, but the scatter of the relations seems larger for group, field and isolated galaxies than for cluster galaxies.

A thorough analysis of the highest signal-to-noise galax-

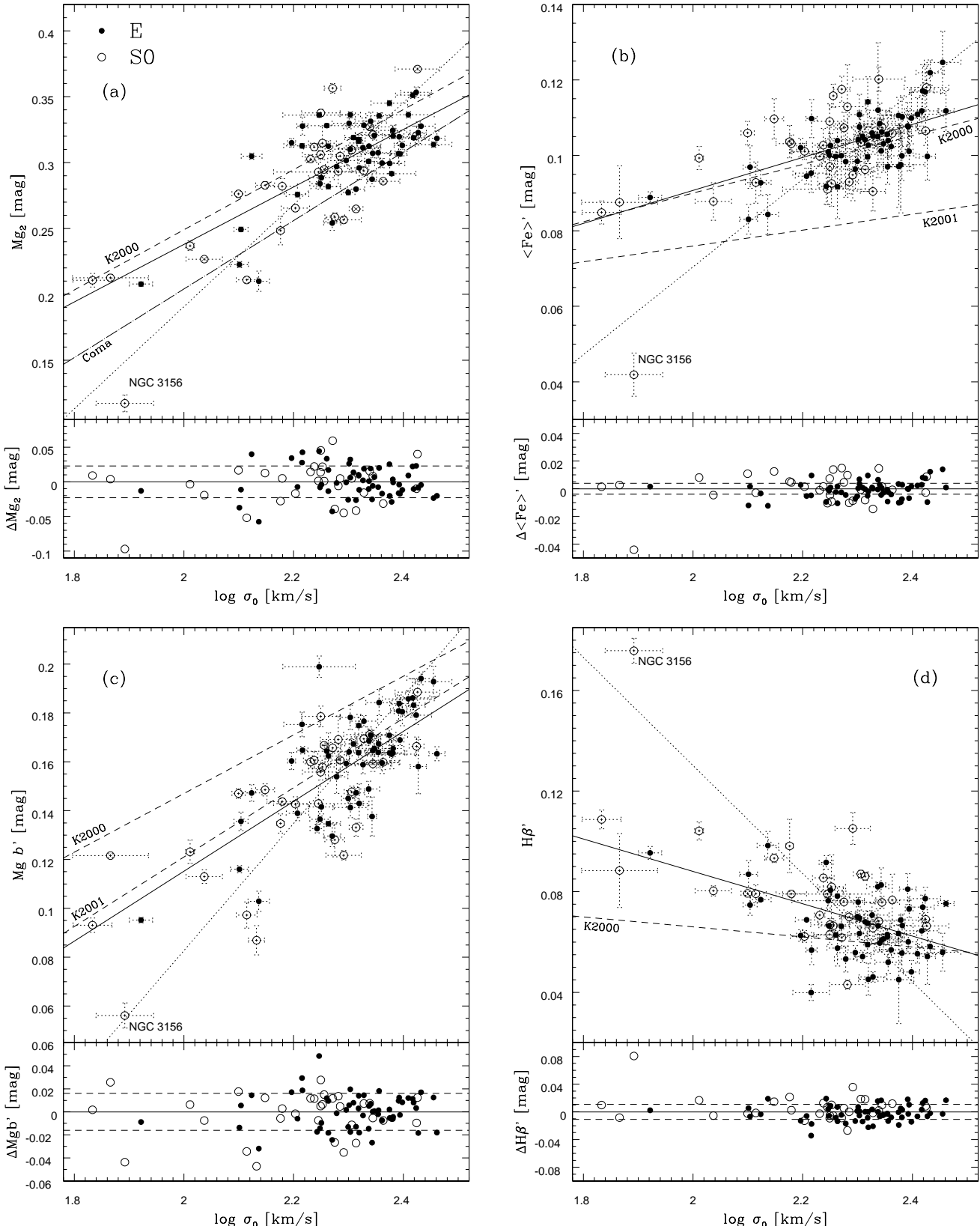


Figure 9. (a)  $Mg_2$  vs  $\log \sigma_0$ ; (b)  $\langle Fe \rangle^0$  vs  $\log \sigma_0$ ; (c)  $Mg b'$  vs  $\log \sigma_0$ ; (d)  $H\beta'$  vs  $\log \sigma_0$  relations. The indices are measured in magnitudes. The dashed line indicates the fit for the cluster sample of Kuntschner (2000, K2000) and the cluster+field sample of Kuntschner et al. (2001, K2001). The dot-dashed line in panel (a) represents the least square bisector fit by Guzman et al. (1992) using a sample of 51 Coma cluster ellipticals. Two fits are shown for our galaxy sample: the solid line is a normal least square fit with the index as dependent variable, and the dotted line is the ordinary least square fit with  $\log \sigma_0$  as dependent variable. The residuals of the relations, shown in the lower panels, are calculated with respect to the solid line fits. The dashed lines in the bottom panels indicate the 1-sigma intrinsic scatter of the residuals.

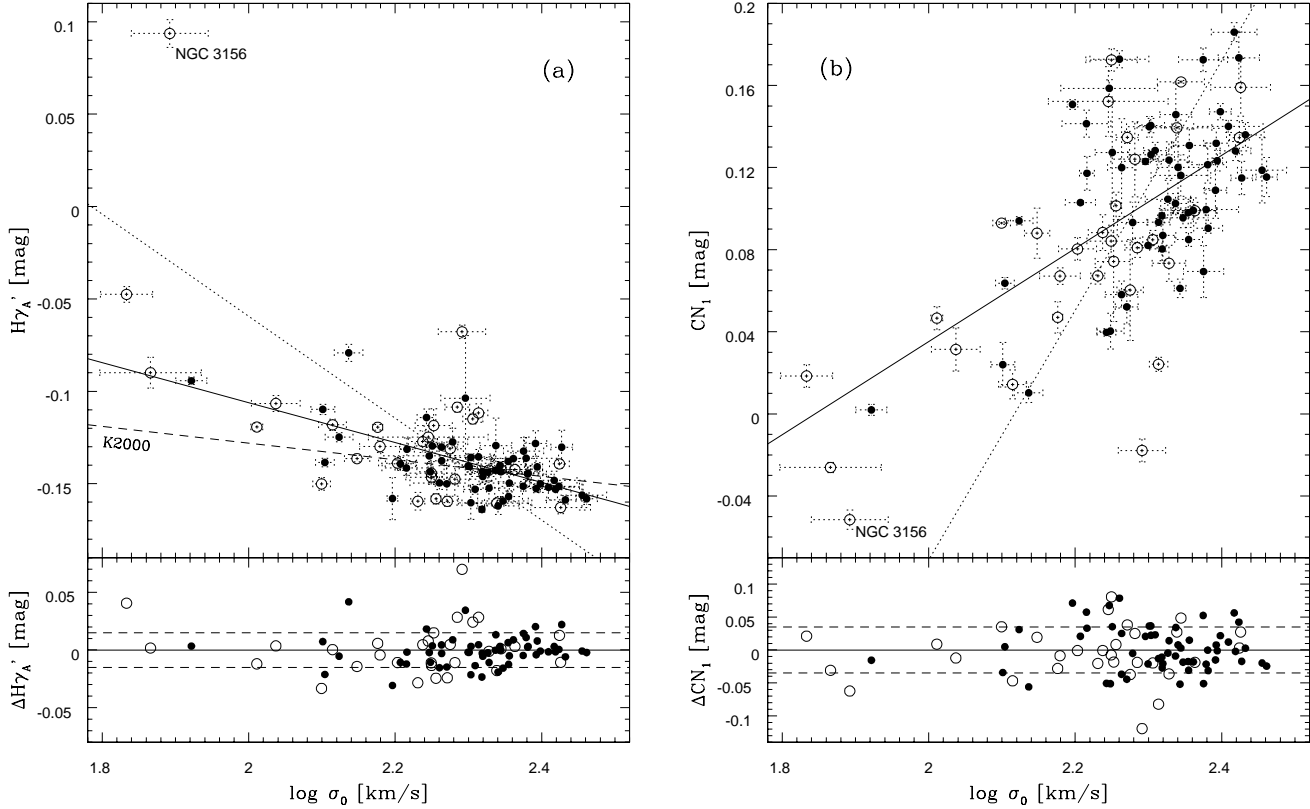


Figure 10. (a)  $H_A^0$  vs  $\log \sigma_0$ ; (b)  $CN_1$  vs  $\log \sigma_0$  relations. The indices are measured in magnitudes. The dashed line indicates the fit for the cluster sample of Kuntschner (2000, K2000). Two fits are shown for our galaxy sample: the solid line is a normal least square fit with the index as dependent variable, and the dotted line is the ordinary least square fit with  $\log \sigma_0$  as dependent variable. The residuals of the relations, shown in the lower panels, are calculated with respect to the solid line fits. The dashed lines in the bottom panels indicate the 1-sigma intrinsic scatter in the residuals.

ies with discussions on the age and metallicity determinations is presented in a forthcoming paper.

#### A C K N O W L E D G E M E N T S

GD would like to thank CNPq-Brazil for the PhD fellowship, INAOE for hospitality during the visits to Mexico, Selwyn College and Cambridge Philosophical Society for financial support. The authors are grateful to the INAOE Committee for telescope time for supporting this project for five consecutive semesters and to the staff at Cananea for cheerful logistic help during the observations. We thank Américo Friaca and Alessandro Bressan for several interesting discussions, Max Pettini and Alfonso Aragon-Salamanca for substantial comments to improve this work, and Ewan O'Sullivan for providing us with the details of the isolated sample selection previous to publication. We also thank an anonymous referee for a very thorough analysis of the manuscript. RJT and ET acknowledge the Mexican Research Council Project grants 40018-A-1 and E32186, respectively.

#### R E F E R E N C E S

- Aeppli C., 1966, ApJS, 14, 1
- Baugh C.M., Cole S., Frenk C.S. & Lacey C.G., 1998, ApJ, 498, 504
- Bender R., Burstein D., Faber S.M., 1993, ApJ, 411, 153
- Bender R., Saglia R.P., Gerhard O.E., 1994, MNRAS, 269, 785
- Berlind A.A., Weinberg D.H., Benson A.J., Baugh C.M., Cole S., Dave R., Frenk C.S., Jenkins A., Katz N. & Lacey C.G., 2003, ApJ, 593, 1
- Bernardi M., Renzini A., da Costa L.N., Wegner G., Alonso M.V., Pellegrini P.S., Rite C., Willmer C.N.A., 1998, ApJ, 508, L43
- Bevington P.R., 1969, Data Reduction and Error Analysis for the Physical Sciences, McGraw-Hill
- Binette L., Magris C.G., Stasinska G., Brzuzual A.G., 1994, A&A, 292, 13
- Bower R.G., Lucey J.R. & Ellis R.S., 1992, MNRAS, 254, 601
- Bower R.G., Terlevich A., Kodama T., Caldwell N., 1998, astro-ph/9808325
- Burstein D., Faber S.M., Gaskell C.M., Krumm N., 1984, ApJ, 287, 586
- Burstein D., Bertola F., Buson L.M., Faber S.M., Lauer T.R., 1988, ApJ, 328, 440
- Buzzoni A., Mantegazza L., Griboudi G., 1994, AJ, 107, 513
- Caldwell N., 1984, PASP, 96, 287
- Cardiel N., Gorgas J., Cenarro J., Gonzalez J.J., 1998, A&AS, 127, 597
- Carrasco L., Buzzoni A., Salsa M., Recillas-Cruz E., 1996, ASP Conf. Ser. 86, 235
- Centeno R. & Ostriker J.P., 1992, ApJ, 399, L113
- Chiosi C. & Carraro G., 2002, MNRAS, 335, 335
- Colbert J.W., Mulchaey J.S., Zabludo A.I., 2001, AJ, 121, 808
- Colina L. & Arrizabalaga S., 1999, ApJ, 514, 637

- Colless M., Burstein D., Davies R. L., McDermah R. K., Saglia R. P., Wegner G., 1999, MNRAS, 303, 813
- Concannon K. D., Rose J. A., Caldwell N., 2000, ApJ, 536, 19
- Covino S., Gallego S., Pasinetti L. E., 1995, A&A, 303, 79
- Davies R. L., Burstein D., Dressler A., Faber S. M., Lynden-Bell D., Terlevich R. J., Wegner G., 1987, ApJS, 64, 581
- de Freitas Pacheco J. A. & Barbuy B., 1995, A&A, 302, 718
- Dressler A., 1984, ApJ, 286, 97
- Faber S. M., Friel E. D., Burstein D., Gaskell C. M., 1985, ApJS, 57, 711
- Filippenko A. & Terlevich R., 1992, ApJ, 397, 79
- Forbes D. A., 1991, MNRAS, 249, 779
- Franx M., Illingworth G., Heckman T., 1989, ApJ, 344, 613
- Garcia A. M., 1993, A&AS, 100, 47
- Gonzalez J. J., 1993, PhD thesis, Univ. California
- Gregg M. D., 1994, AJ, 108, 2164
- Guzman R., Lucey J. R., Carter D., Terlevich R. J., 1992, MNRAS, 257, 187
- Isobe T., Feigelson E. D., Akritas M. G., Babu G. J., 1990, ApJ, 364, 104
- Jones L. A. & Worthey G., 1995, ApJ, 446, L31
- Jørgensen I., Franx M. & Kajrgaard P., 1995, MNRAS, 276, 1341
- Jørgensen I., 1997, MNRAS, 288, 161
- Kaumann G. & Charlot S., 1998, MNRAS, 297, 23
- Kaumann G., Colberg J. M., Diaferio A. & White S. D. M., 1999, MNRAS, 303, 188
- Kaumann G., White S. D. M., Heckman T. M., Menard B., Brinchmann J., Charlot S., Tremonti C., & Brinkmann J., 2004, MNRAS, 353, 713
- Kay S. T., Pearce F. R., Frenk C. S. & Jenkins A., 2002, MNRAS, 330, 113
- Kuntschner H., 1998, PhD thesis, Univ. of Durham
- Kuntschner H. & Davies R. L., 1998, MNRAS, 295, 29
- Kuntschner H., 2000, MNRAS, 315, 184
- Kuntschner H., Lucey J. R., Smith R. J., Hudson M. J. & Davies R. L., 2001, MNRAS, 323, 615
- Kuntschner H., Smith R. J., Colless M., Davies R. L., Kaldare R., Vazdekis, A., 2002, MNRAS, 337, 172
- Mastaston C. & Thomas D., 2000, ApJ, 541, 126
- Mastaston C., GREGGIO L., Renzini A., Orlonani S., Saglia R. P., Puzia T. H., Kissler-Patig M., 2003, A&A, 400, 823
- Oke J. B., 1990, AJ, 99, 1621
- Osterbrock D. E., 1989, Astrophysics of Gaseous Nebulae and Active Galactic Nuclei, University Science Books
- Pearce F. R., Jenkins A., Frenk C. S., Colberg J. M., White S. D. M., Thomas P. A., Couchman H. M. P., Peacock J. A., Efstathiou G. & The Virgo Consortium, 1999, ApJ, 521, L99
- Peterson R. C., Camey B. W., Dorman B., Green E. M., Lansdowne W., Liebert J., O'Connell R. W., Rood R. T., 2003, ApJ, 588, 299
- Phillips M. M., Jenkins C. R., Dopita M. A., Sadler E. M., Binette L., 1986, AJ, 92, 503
- Pugnelli P. & Simien F., 1996, A&A, 309, 749 (PS96)
- Renda F., Forbes D. A., O'Sullivan E., Goudrooij P., 2004, submitted to MNRAS
- Somerville R. S., & Primack J. R., 1999, MNRAS, 310, 1087
- Terlevich R., Davies R. L., Faber S. M., Burstein D., 1981, MNRAS, 196, 381
- Terlevich A. J. & Forbes D., 2002, MNRAS, 330, 547 (TF02)
- Thomas D., Mastaston C. & Bender R., 2003, MNRAS, 339, 897 (TM03)
- Tonry J. & Davies M., 1981, ApJ, 246, 666
- Trager S. C., 1997, PhD Thesis, Univ. of California, Santa Cruz
- Trager S. C., Worthey G., Faber S. M., Burstein D. & Gonzalez J. J., 1998, ApJS, 166, 1
- Trager S. C., Faber S. M., Worthey G., Gonzalez J. J., 2000, AJ, 119, 1645 (2000a)

- Trager S. C., Faber S. M., Worthey G., Gonzalez J. J., 2000, AJ, 120, 165 (2000b)
- Tran H. D., Svetanov Z., Ford H. C., Davies J., Lawrence, van den Bosch F. C., Rest A., 2001, AJ, 121, 2928
- Tully R. B., 1987, Nearby Galaxy Catalog (Cambridge: Cambridge University Press)
- White S. D. M. & Rees M. J., 1978, MNRAS, 183, 341
- Willis J. P., Hewett P. C., Warren S. J., Lewis G. F., 2002, MNRAS, 337, 953
- Worthey G., Faber S. M., Gonzalez J. J. & Burstein D., 1994, ApJS, 94, 687
- Worthey G., 1994, ApJS, 95, 107 (W94)
- Worthey G. & Ottaviani D. L., 1997, ApJS, 111, 377
- Worthey G. & Colber M., 2003, ApJ, 586, 17

#### APPENDIX A : SAMPLE COMPLEMENTARY INFORMATION

Table A1 contains complementary information about the galaxy sample, including environment information and our classification as group, field and isolated galaxy.

#### APPENDIX B : FULLY CORRECTED LICK-STRENGTH INDEXES

We present the final corrected central  $r_e/8$  index measurements and associated errors for our galaxy sample. The Lick indices presented in Table B1 were calibrated to the Lick/IDS system, and corrected for velocity dispersion and nebular emission (in this case mainly the Balmer lines).

Table A 1. Complementary details of the galaxy sample.

Name	Type	$V_{\text{rot}}$ (km/s)	$r_e$ (")	$\log R_{25}$	$\text{PA}_{\text{maj}}$ ( $^{\circ}$ )	$F_{\text{P}_{\text{res}}}$	Environment information
ESO 462-G 015	-5	-	21	0.11	166	-0.05	Isolated
MCG -01-03-018	-3	-	23*	0.00		0.29	Isolated
NGC 0016	-3	160	28*	0.27	16	0.02	Field
NGC 0221	-6	46	36	0.13	170	0.19	M 32, dwarf companion of M 31, group (LGG 11)
NGC 0315	-4	32	37	0.20	40	0.09	Group (LGG 14)
NGC 0474	-2	-	34	0.05	75	0.11	Ap227, group (LGG 20)
NGC 0584	-5	157	25	0.26	55	-0.28	Group (LGG 27)
NGC 0720	-5	48	36	0.29	140	0.02	Group (LGG 38)
NGC 0750	-5	40	27*	0.10		0.04	Ap166, pair with NGC 0751, group (LGG 42)
NGC 0751	-5	-	22*	0.00		0.20	Ap166, pair with NGC 0750, group (LGG 42)
NGC 0777	-5	53	34	0.08	155	0.15	Group (LGG 42)
NGC 0821	-5	89	50	0.20	25	0.28	Isolated
NGC 0890	-3	-	34	0.16	50*	-0.17	Field
NGC 1045	-3	-	36*	0.28	40	0.19	Isolated
NGC 1052	-5	101	34	0.16	120	0.32	Group (LGG 71)
NGC 1132	-4.5	-	34	0.27	140	0.06	Isolated
NGC 1407	-5	30	70	0.03	35	0.21	Eridanus group (LGG 100)
NGC 1453	-5	-	25	0.09		0.29	Group (LGG 103)
NGC 1600	-5	4	45	0.17	15	0.20	Field
NGC 1700	-5	75	18	0.20	90	-0.51	Group (LGG 123)
NGC 1726	-2	40	24	0.12	170	-0.10	Field
NGC 2128	-3	-	23*	0.13	60	0.51	Isolated
NGC 2300	-2	6	31	0.14		0.44	Ap114, group (LGG 145)
NGC 2418	-5	142	28*	0.00		0.31	Ap165, field
NGC 2513	-5	53	33	0.09	170	0.19	Field
NGC 2549	-2	115	17	0.48	177	-0.03	Field
NGC 2768	-5	78	64	0.28	95	-0.06	Group (LGG 167)
NGC 2872	-5	75	18	0.06	22	0.17	Ap307, field
NGC 2911	-2	-	51	0.11	140	0.17	Ap232, group (LGG 177)
NGC 2974	-5	202	24	0.23	40	0.21	Group (LGG 179)
NGC 3091	-5	71	33	0.20	149	0.27	Group (LGG 186)
NGC 3098	-2	130	15	0.57	90	-0.12	Field
NGC 3115	-3	273	32	0.47	40	-0.11	Field
NGC 3139	-2	-	22*	0.08		1.46	Field
NGC 3156	-2	79	14	0.24	47	-0.54	Group (LGG 192)
NGC 3193	-5	80	27	0.05		0.26	Ap316, group (LGG 194)
NGC 3226	-5	40	34	0.05	15	0.40	Ap094, group (LGG 194)
NGC 3245	-2	-	27	0.26	177	0.09	Group (LGG 197)
NGC 3377	-5	86	34	0.24	35	0.03	Leo group (LGG 217)
NGC 3379	-5	53	35	0.05		-0.18	Leo group (LGG 217)
NGC 3384	-3	-	25	0.34	53	-0.23	Leo group (LGG 217)
NGC 3412	-2	-	26	0.25	155	-0.38	Leo group (LGG 217)
NGC 3414	-2	63	21	0.14		0.18	Ap162, group (LGG 227)
NGC 3599	-2	-	24	0.10		-0.12	Field
NGC 3607	-2	108	43	0.30	120	0.22	Field
NGC 3608	-5	26	34	0.09	75	0.27	Group (LGG 237)
NGC 3610	-5	143	15	0.07		-0.50	Group (LGG 234)
NGC 3613	-5	141	27	0.32	102	-0.04	Group (LGG 232)
NGC 3636	-5	-	20*	0.00		-0.04	Group (LGG 235)
NGC 3640	-5	114	32	0.10	100	0.00	Group (LGG 233)
NGC 3665	-2	103	29	0.08	30	0.00	Group (LGG 236)
NGC 3923	-5	-	50	0.18	50	0.01	Group (LGG 255)
NGC 3941	-2	-	23	0.18	10	-0.39	Field
NGC 4125	-5	97	58	0.26	95	0.05	Group (LGG 274)
NGC 4261	-5	69	36	0.05	160	0.13	3C 270, group (LGG 278)
NGC 4365	-5	43	50	0.14	40	0.04	Virgo, group (LGG 289)
NGC 4374	-5	23	51	0.06	135	0.08	Virgo, group (LGG 292)
NGC 4494	-5	67	49	0.13		-0.33	Group (LGG 294)
NGC 4550	-1.5	122	15	0.55	178	-0.03	Field
NGC 4754	-3	89	26	0.27	23	-0.08	Virgo, group (LGG 289)
NGC 5322	-5	20	34	0.18	95	-0.07	Group (LGG 360)
NGC 5353	-2	-	15	0.30	145	0.03	Group (LGG 363)
NGC 5354	-2	-	18	0.04		-0.14	Group (LGG 361)

Table A 1.C continued.

Name	Type	$V_{\text{rot}}$ (km/s)	$r_e$ (")	$\log R_{25}$	$\text{PA}_{\text{maj}}$ (°)	$F_{\text{P}}_{\text{res}}$	Environment information
NGC 5363	90.0	—	36	0.19	135	0.06	Group (LGG 362)
NGC 5444	-4	—	27	0.06	90	0.17	Group (LGG 370)
NGC 5557	-5	—	30	0.09	105	-0.04	Group (LGG 378)
NGC 5576	-5	14	18	0.20	95	-0.14	Group (LGG 379)
NGC 5638	-5	62	28	0.05	150	-0.01	Group (LGG 386)
NGC 5812	-5	40	26	0.06	—	0.24	Field
NGC 5813	-5	36	57	0.14	145	0.23	Group (LGG 393)
NGC 5831	-5	27	26	0.04	55	0.24	Group (LGG 393)
NGC 5845	-4.6	127	12*	0.19	150	0.81	Group (LGG 392)
NGC 5846	-5	4	62	0.03	—	0.12	Pair with NGC 5846A, group (LGG 393)
NGC 5846 A	-6	74	6*	0.15	120	0.35	Pair with NGC 5846, group (LGG 393)
NGC 5854	-1	—	15	0.54	55	-0.24	Group (LGG 393)
NGC 5864	-2	—	44*	0.49	68	0.24	Group (LGG 393)
NGC 5869	-2	—	36*	0.14	125	0.32	Group (LGG 393)
NGC 5982	-5	45	24	0.12	110	0.00	Group (LGG 402)
NGC 6172	-4	—	16*	0.00	—	-0.12	Isolated
NGC 6411	-5	14	29	0.10	70	-0.18	Isolated
NGC 7302	-3	—	13	0.21	100*	0.15	Field
NGC 7332	-2	134	15	0.56	155	-0.30	Field
NGC 7454	-5	23	25	0.15	150	-0.07	Group (LGG 469)
NGC 7585	-1	—	24	0.07	105	-0.09	Ap223, old
NGC 7619	-5	69	37	0.04	30	0.29	Pegasus I group (LGG 473)
NGC 7626	-5	20	39	0.05	—	0.25	Pegasus I group (LGG 473)

References: Morphologies are from the Third Reference Catalogue (RC3). The maximum rotation velocity  $V_{\text{rot}}$  is from Prugniel & Simien (1996). Effective radius  $r_e$  and the  $R_{25}$  parameter are from Trager et al. (2000b) and RC3 catalog. The Fundamental Plane residual  $F_{\text{P}}_{\text{res}}$  was derived from eq.(4) in Prugniel & Simien (1996). The asterisk symbols assign estimates made by the authors. Environmental information is from E. O'Sullivan (private communication); the group identification was extracted from Garcia 1993 (LGG group number in parenthesis).

Galaxy	H $\delta_A$ [Å]	H $\delta_F$ [Å]	H $\gamma_A$ [Å]	H $\gamma_F$ [Å]	CN <sub>1</sub> [mag]	CN <sub>2</sub> [mag]	Ca4227 [Å]	G4300 [Å]	Fe4383 [Å]	Ca4455 [Å]	Fe4531 [Å]	C <sub>2</sub> 4668 [Å]	H $\beta$ [Å]	Fe5015 [Å]	Mg <sub>1</sub> [mag]	Mg <sub>2</sub> [mag]	Mg <sub>b</sub> [Å]	Fe5270 [Å]	Fe5335 [Å]	Fe5406 [Å]	Fe5709 [Å]	Fe5782 [Å]	NaD [Å]	TiO <sub>1</sub> [mag]	TiO <sub>2</sub> [mag]
ESO462-G015	-2.40	0.15	-5.85	-1.43	0.100	0.143	1.47	5.44	5.31	1.79	3.58	8.21	1.76	4.66	0.104	0.292	4.53	2.73	3.40	1.87	0.79	1.29	4.77	0.040	0.070
±	0.30	0.43	0.55	0.44	0.011	0.016	0.20	0.21	0.45	0.14	0.18	0.18	0.05	0.25	0.005	0.001	0.16	0.44	0.25	0.35	0.15	0.31	0.28	0.002	0.006
MCG01-03-018	-3.21	-0.57	-6.37	-1.43	0.124	0.165	1.29	5.57	6.53	1.78	4.30	8.23	1.12	5.16	0.112	0.293	4.69	3.34	3.37	1.82	0.95	1.07	5.14	0.065	0.096
±	0.49	0.41	0.52	0.34	0.018	0.021	0.07	0.50	0.61	0.41	0.16	0.57	0.05	0.23	0.004	0.011	0.24	0.18	0.15	0.11	0.09	0.14	0.10	0.005	0.003
NGC 0016	-1.68	0.62	-5.56	-1.23	0.067	0.111	1.16	5.18	5.93	1.64	3.62	8.47	2.02	5.89	0.121	0.282	4.03	3.30	2.92	1.71	0.94	1.25	4.42	0.032	0.074
±	0.24	0.15	0.17	0.03	0.006	0.006	0.07	0.05	0.17	0.07	0.20	0.37	0.02	0.18	0.001	0.006	0.07	0.11	0.06	0.11	0.11	0.07	0.09	0.000	0.001
NGC 0221	-0.90	1.01	-3.97	-0.37	0.002	0.036	1.07	4.76	4.87	1.31	3.18	5.92	2.42	5.81	0.092	0.207	2.73	3.02	2.60	1.56	1.00	0.95	3.25	0.047	0.056
±	0.08	0.02	0.09	0.07	0.003	0.002	0.01	0.09	0.11	0.04	0.05	0.19	0.06	0.18	0.005	0.005	0.05	0.05	0.06	0.05	0.01	0.02	0.09	0.001	0.001
NGC 0315	-2.49	0.27	-5.48	-0.93	0.109	0.152	1.31	5.49	5.93	1.87	4.01	8.37	2.01	4.42	0.141	0.307	4.99	3.46	3.23	1.95	0.93	1.40	5.28	0.045	0.078
±	0.48	0.16	0.34	0.19	0.014	0.014	0.09	0.10	0.23	0.17	0.24	0.40	0.17	0.29	0.008	0.008	0.10	0.14	0.17	0.20	0.03	0.14	0.18	0.002	0.002
NGC 0474	-2.41	0.36	-5.97	-1.38	0.080	0.118	1.32	5.45	5.77	1.64	4.01	6.44	1.71	6.03	0.115	0.266	4.00	3.25	2.89	2.05	0.83	0.95	4.11	0.050	0.101
±	0.17	0.06	0.17	0.10	0.005	0.009	0.11	0.03	0.07	0.10	0.25	0.30	0.10	0.27	0.003	0.008	0.01	0.10	0.09	0.13	0.09	0.15	0.001	0.002	
NGC 0584	-2.38	0.38	-6.04	-1.45	0.082	0.121	1.19	5.51	5.49	1.48	3.73	8.08	1.90	6.43	0.122	0.277	4.06	3.34	2.76	1.75	1.00	1.03	4.06	0.042	0.082
±	0.07	0.14	0.22	0.14	0.002	0.004	0.06	0.10	0.14	0.05	0.09	0.23	0.10	0.05	0.007	0.002	0.09	0.09	0.04	0.03	0.05	0.10	0.002	0.000	
NGC 0720	-3.40	-0.05	-6.40	-1.70	0.186	0.244	1.50	5.28	6.63	1.78	3.74	9.40	1.74	5.81	0.174	0.351	5.12	3.56	2.97	1.77	0.80	1.08	6.10	0.051	0.095
±	0.20	0.12	0.23	0.07	0.005	0.004	0.07	0.27	0.11	0.08	0.22	0.59	0.18	0.44	0.001	0.002	0.18	0.15	0.09	0.07	0.05	0.10	0.07	0.002	0.002
NGC 0750	-2.67	-0.16	-5.45	-1.01	0.093	0.134	1.08	5.59	4.60	1.26	4.19	8.29	1.38	4.58	0.119	0.297	4.30	3.55	3.24	1.77	0.75	1.26	5.14	0.048	0.076
±	0.54	0.17	0.35	0.16	0.010	0.014	0.26	0.21	0.56	0.16	0.12	0.36	0.12	0.23	0.004	0.004	0.17	0.04	0.13	0.07	0.18	0.07	0.09	0.003	0.003
NGC 0751	-1.73	0.00	-6.49	-1.57	0.052	0.090	0.95	6.14	5.81	1.05	4.15	7.48	1.70	3.61	0.096	0.254	3.66	3.42	2.57	2.05	0.79	1.33	3.45	0.037	0.066
±	0.57	0.38	0.50	0.26	0.009	0.014	0.17	0.19	0.39	0.08	0.38	0.37	0.09	0.34	0.002	0.006	0.11	0.18	0.23	0.06	0.04	0.08	0.10	0.002	0.002
NGC 0777	-2.62	-0.11	-5.58	-1.32	0.115	0.168	0.99	4.91	5.12	1.52	4.40	10.33	1.40	4.18	0.154	0.322	4.40	3.50	3.03	1.72	0.92	1.18	5.98	0.063	0.110
±	0.51	0.14	0.45	0.24	0.010	0.014	0.17	0.28	0.15	0.05	0.19	0.20	0.26	0.11	0.002	0.008	0.27	0.16	0.24	0.17	0.10	0.09	0.11	0.002	0.003
NGC 0821	-2.76	0.18	-6.20	-1.50	0.104	0.149	1.31	5.36	6.22	1.59	3.75	8.34	1.81	5.44	0.149	0.311	4.42	3.15	3.12	1.75	0.79	1.00	4.46	0.054	0.100
±	0.33	0.17	0.23	0.15	0.009	0.007	0.11	0.24	0.17	0.05	0.15	0.41	0.14	0.07	0.007	0.005	0.09	0.09	0.10	0.09	0.11	0.02	0.03	0.001	0.000
NGC 0890	-1.01	0.74	-4.74	-0.93	0.024	0.058	0.77	4.65	4.97	1.42	4.13	8.50	2.19	6.36	0.104	0.265	3.75	3.32	2.97	1.88	1.06	4.48	4.24	0.045	0.096
±	0.15	0.12	0.24	0.12	0.004	0.007	0.34	0.10	0.30	0.13	0.12	0.47	0.04	0.81	0.001	0.001	0.09	0.16	0.06	0.17	0.08	0.05	0.03	0.002	0.001
NGC 1045	-2.71	0.26	-6.12	-1.57	0.099	0.149	1.44	5.35	5.56	1.58	3.99	8.01	1.94	5.58	0.117	0.286	4.45	3.56	3.24	1.94	0.94	0.98	5.07	0.059	0.104
±	0.10	0.13	0.13	0.14	0.005	0.003	0.09	0.10	0.14	0.09	0.12	0.17	0.26	0.33	0.003	0.002	0.08	0.06	0.14	0.09	0.04	0.06	0.05	0.001	0.004
NGC 1052	-0.45	1.64	-5.72	-0.62	0.158	0.205	1.12	5.77	6.25	1.59	3.60	7.37	1.85	2.50	0.182	0.336	5.44	2.85	2.89	1.83	0.88	1.03	6.28	0.062	0.112
±	0.58	0.50	0.57	0.48	0.005	0.009	0.13	0.29	0.11	0.07	0.12	0.11	0.41	0.09	0.001	0.002	0.12	0.06	0.04	0.04	0.02	0.05	0.06	0.001	0.001
NGC 1132	-2.05	0.51	-5.68	-1.19	0.070	0.109	0.91	5.22	6.07	1.55	3.19	6.53	1.16	3.56	0.133	0.299	4.55	2.63	2.84	1.62	0.83	1.01	4.12	0.044	0.065
±	0.67	0.55	0.37	0.22	0.014	0.008	0.27	0.05	0.63	0.24	0.25	0.64	0.42	0.37	0.004	0.008	0.12	0.09	0.16	0.14	0.06	0.08	0.10	0.003	0.002
NGC 1407	-2.92	-0.18	-6.55	-1.88	0.173	0.232	1.71	5.65	6.64	1.79	3.51	8.78	1.96	5.89	0.178	0.353	4.94	3.65	3.37	1.78	0.83	1.23	5.73	0.068	0.110
±	0.50	0.25	0.09	0.14	0.013	0.012	0.14	0.10	0.27	0.15	0.35	0.33	0.13	0.26	0.005	0.004	0.09	0.14	0.18	0.13	0.08	0.06	0.05	0.002	0.003
NGC 1453	-3.51	0.17	-6.48	-1.73	0.148	0.204	1.43	5.52	5.76	1.88	4.01	9.43	1.21	4.44	0.138	0.313	4.98	3.72	3.32	1.94	0.98	0.95	5.70	0.052	0.121
±	0.29	0.25	0.26	0.11	0.009	0.007	0.17	0.29	0.25	0.14	0.12	0.54	0.13	0.15	0.005	0.003	0.17	0.28	0.12	0.14	0.04	0.08	0.15	0.002	0.003
NGC 1600	-3.33	0.11	-6.62	-1.73	0.128	0.189	1.53	5.65	6.65	1.84	4.12	9.95	1.87	5.87	0.142	0.319	5.05	3.51	3.54	2.18	0.82	1.61	6.15	0.055	0.063
±	0.13	0.33	0.09	0.14	0.008	0.010	0.16	0.11	0.19	0.07	0.19	0.21	0.13	0.24	0.004	0.001	0.10	0.15	0.27	0.06	0.19	0.16	0.31	0.001	0.001
NGC 1700	-1.38	0.66	-6.03	-1.25	0.062	0.101	0.78	5.71	6.03	1.39	3.72	8.72	2.10	5.52	0.122	0.288	3.87	3.16	2.79	1.79	0.98	0.85	4.89	0.051	0.092
±	0.34	0.29	0.06	0.10	0.006	0.003	0.03	0.18	0.17	0.09	0.35	0.09	0.18	0.38	0.002	0.005	0.21	0.08	0.08	0.05	0.01	0.03	0.05	0.003	0.006
NGC 1726	-2.34	0.27	-6.14	-1.67	0.074	0.124	1.27	5.17	4.91	1.60	3.58	8.24	1.67	5.06	0.126	0.294	4.70	3.00	2.75	1.69	0.91	0.80	4.39	0.051	0.106
±	0.33	0.27	0.28	0.07	0.010	0.011	0.12	0.29	0.22	0.19	0.06	0.24	0.18	0.22	0.002	0.003	0.09	0.17	0.12	0.11	0.08	0.05	0.08	0.002	0.005
NGC 2128	-0.69	1.17	-5.03	-0.66	0.075	0.116	1.41	5.13																	

Table B 1. Fully corrected Lick/IDS indices for the central  $z=8$  extraction: continued.

Galaxy	$H\delta_A$ [Å]	$H\delta_F$ [Å]	$H\gamma_A$ [Å]	$H\gamma_F$ [Å]	CN <sub>1</sub> [mag]	CN <sub>2</sub> [mag]	Ca4227 [Å]	G4300 [Å]	Fe4383 [Å]	Ca4455 [Å]	Fe4531 [Å]	C <sub>2</sub> 4668 [Å]	$H\beta$ [Å]	Fe5015 [Å]	Mg <sub>1</sub> [mag]	Mg <sub>2</sub> [mag]	Mg <sub>b</sub> [Å]	Fe5270 [Å]	Fe5335 [Å]	Fe5406 [Å]	Fe5709 [Å]	Fe5782 [Å]	NaD [Å]	TiO <sub>1</sub> [mag]	TiO <sub>2</sub> [mag]	
NGC 2513	-3.13	0.81	-6.61	-1.85	0.132	0.179	1.23	5.49	6.11	1.90	3.86	9.23	1.63	5.30	0.150	0.319	5.06	3.63	2.89	1.99	1.10	0.92	5.53	0.034	0.091	
±	0.37	0.20	0.11	0.06	0.008	0.007	0.09	0.14	0.17	0.12	0.15	0.18	0.11	0.22	0.002	0.004	0.09	0.10	0.17	0.09	0.11	0.10	0.12	0.004	0.003	
NGC 2549	-2.29	0.67	-5.86	-1.02	0.088	0.124	1.33	5.25	6.36	1.60	3.79	9.07	2.36	5.93	0.125	0.283	4.16	3.52	3.02	1.91	0.97	1.07	4.31	0.044	0.108	
±	0.29	0.04	0.08	0.05	0.012	0.011	0.09	0.16	0.31	0.05	0.10	0.63	0.13	0.18	0.001	0.003	0.07	0.08	0.11	0.05	0.19	0.04	0.07	0.001	0.004	
NGC 2768 0°	-2.17	0.47	-6.21	-1.50	0.084	0.122	1.20	5.34	6.37	1.64	3.61	7.22	1.61	4.83	0.146	0.306	4.34	3.44	3.02	1.50	0.96	0.90	3.83	0.031	0.081	
±	0.16	0.17	0.31	0.25	0.008	0.014	0.13	0.11	0.14	0.18	0.13	0.15	0.12	0.12	0.002	0.003	0.08	0.11	0.18	0.09	0.21	0.13	0.13	0.001	0.003	
NGC 2768 90°	-2.40	0.38	-6.85	-1.75	0.102	0.143	1.30	5.54	6.75	1.79	4.11	7.33	1.69	5.45	0.123	0.295	4.63	3.66	3.18	2.02	—	—	—	—	—	—
±	0.14	0.12	0.14	0.13	0.007	0.008	0.09	0.11	0.13	0.01	0.07	0.34	0.07	0.13	0.003	0.002	0.01	0.05	0.09	0.09	—	—	—	—	—	—
NGC 2872	-2.18	0.60	-6.24	-1.79	0.121	0.175	1.38	5.22	5.32	1.76	4.32	8.16	1.54	5.44	0.158	0.325	4.55	3.26	3.13	1.54	1.00	1.20	5.18	0.028	0.086	
±	0.23	0.29	0.21	0.08	0.010	0.011	0.21	0.12	0.32	0.13	0.19	0.30	0.20	0.17	0.003	0.004	0.09	0.15	0.12	0.11	0.10	0.13	0.14	0.002	0.004	
NGC 2911	0.64	2.15	-5.40	-0.64	0.088	0.126	1.24	4.61	6.50	1.38	3.11	6.91	2.12	4.68	0.170	0.312	4.47	2.84	2.87	1.75	0.94	0.89	6.25	0.047	0.091	
±	0.52	0.37	0.40	0.31	0.010	0.012	0.15	0.13	0.27	0.30	0.29	0.61	0.26	0.20	0.003	0.002	0.10	0.10	0.09	0.11	0.07	0.07	0.07	0.003	0.002	
NGC 2974	-2.64	0.56	-4.42	-0.71	0.123	0.166	1.18	5.26	5.44	1.46	3.44	7.92	1.41	4.43	0.143	0.301	4.43	3.10	2.83	2.04	1.00	0.99	4.80	0.036	0.095	
±	0.12	0.15	1.53	0.79	0.002	0.003	0.09	0.04	0.32	0.01	0.10	0.24	0.10	0.10	0.001	0.004	0.09	0.08	0.10	0.06	0.12	0.05	0.05	0.003	0.004	
NGC 3091	-2.69	0.17	-6.77	-1.79	0.119	0.175	1.85	5.26	6.44	1.69	4.43	9.60	1.43	6.34	0.146	0.314	5.29	3.89	4.09	2.01	0.96	1.18	5.52	0.028	0.108	
±	0.37	0.13	0.39	0.20	0.017	0.014	0.30	0.29	0.22	0.18	0.26	0.23	0.19	0.27	0.003	0.002	0.15	0.25	0.22	0.19	0.08	0.31	0.14	0.005	0.002	
NGC 3098	-0.46	0.79	-4.51	-0.79	0.032	0.081	1.16	4.50	4.74	1.43	3.90	5.52	2.05	5.09	0.096	0.227	3.21	3.16	2.44	1.75	1.05	0.94	2.49	0.050	0.069	
±	0.32	0.22	0.19	0.20	0.011	0.013	0.09	0.15	0.23	0.16	0.08	0.19	0.12	0.17	0.002	0.001	0.08	0.18	0.10	0.11	0.03	0.00	0.06	0.002	0.000	
NGC 3115	-3.17	0.01	-6.97	-1.74	0.139	0.187	1.65	5.27	7.01	1.97	3.97	8.45	1.85	6.70	0.158	0.327	4.74	3.62	3.44	1.73	0.94	1.03	5.14	0.050	0.108	
±	0.24	0.18	0.12	0.06	0.001	0.001	0.04	0.17	0.16	0.09	0.04	0.11	0.09	0.10	0.003	0.003	0.06	0.06	0.08	0.05	0.04	0.12	0.001	0.001		
NGC 3139	—	—	—	—	—	—	—	—	—	—	—	—	—	—	—	—	—	—	—	—	—	—	—	—	—	
±	—	—	—	—	—	—	—	—	—	—	—	—	—	—	—	—	—	—	—	—	—	—	—	—	—	
NGC 3156	5.13	4.38	3.61	3.68	-0.051	-0.008	0.44	1.54	1.28	0.54	2.62	2.13	4.29	3.58	0.040	0.117	1.64	1.90	1.63	1.14	0.57	0.38	1.72	0.022	0.024	
±	0.21	0.15	0.28	0.16	0.005	0.003	0.15	0.21	0.15	0.10	0.30	0.31	0.14	0.32	0.004	0.006	0.15	0.30	0.10	0.08	0.08	0.12	0.16	0.004	0.003	
NGC 3193	-2.55	0.09	-6.18	-1.58	0.116	0.164	1.36	5.22	5.91	1.71	4.09	8.25	1.66	5.36	0.139	0.307	4.57	3.47	3.09	1.91	1.05	1.09	4.66	0.049	0.097	
±	0.11	0.06	0.26	0.14	0.010	0.014	0.06	0.12	0.18	0.09	0.21	0.12	0.10	0.05	0.001	0.003	0.12	0.07	0.04	0.10	0.03	0.02	0.05	0.001	0.001	
NGC 3226	-1.34	0.88	-6.07	-1.47	0.142	0.178	1.14	4.66	6.04	1.28	3.72	7.20	1.01	4.02	0.153	0.313	4.85	2.87	2.46	1.68	1.07	1.10	4.93	0.037	0.086	
±	0.39	0.31	0.23	0.14	0.007	0.005	0.05	0.21	0.23	0.08	0.06	0.14	0.13	0.13	0.002	0.002	0.13	0.14	0.12	0.08	0.12	0.08	0.13	0.002	0.002	
NGC 3245	-1.03	0.94	-4.59	-0.57	0.081	0.122	1.04	4.74	5.53	1.60	3.39	8.03	1.77	5.22	0.158	0.305	4.47	2.95	2.55	1.71	0.97	0.88	4.36	0.029	0.092	
±	0.15	0.11	0.16	0.11	0.006	0.005	0.06	0.05	0.13	0.08	0.12	0.21	0.09	0.09	0.002	0.006	0.16	0.04	0.14	0.05	0.12	0.09	0.16	0.003	0.002	
NGC 3377	-1.76	0.58	-5.33	-1.05	0.094	0.138	1.00	5.07	5.43	1.29	3.35	7.39	1.96	5.26	0.150	0.305	4.12	2.97	2.60	1.75	0.90	0.89	4.13	0.031	0.084	
±	0.06	0.06	0.12	0.07	0.003	0.002	0.03	0.11	0.16	0.08	0.10	0.13	0.01	0.07	0.002	0.002	0.09	0.03	0.14	0.12	0.05	0.05	0.07	0.002	0.001	
NGC 3379 90°	-2.95	0.04	-6.63	-1.73	0.129	0.178	1.34	5.42	6.18	1.80	3.88	7.95	1.50	6.41	0.162	0.319	4.64	3.13	3.09	1.91	0.95	1.03	5.05	0.052	0.102	
±	0.08	0.04	0.13	0.08	0.005	0.005	0.05	0.06	0.12	0.07	0.07	0.06	0.10	0.16	0.003	0.002	0.05	0.05	0.04	0.03	0.03	0.06	0.002	0.001		
NGC 3379 70°	-2.64	0.13	-7.13	-2.03	0.097	0.138	1.40	5.63	6.50	1.60	3.80	8.64	1.51	5.81	0.162	0.317	4.75	2.97	2.42	1.89	1.00	1.13	4.76	0.049	0.088	
±	0.08	0.19	0.07	0.02	0.004	0.004	0.05	0.08	0.10	0.02	0.06	0.17	0.12	0.08	0.001	0.001	0.08	0.07	0.02	0.10	0.05	0.02	0.04	0.001	0.003	
NGC 3384	-2.39	0.56	-6.92	-1.82	0.067	0.101	1.26	5.56	6.57	1.50	3.71	9.60	1.81	6.63	0.149	0.302	4.45	2.08	3.27	1.91	1.12	1.13	5.08	0.044	0.085	
±	0.08	0.07	0.23	0.09	0.004	0.005	0.03	0.16	0.16	0.10	0.06	0.17	0.07	0.13	0.002	0.002	0.07	0.05	0.05	0.02	0.05	0.06	0.006	0.004		
NGC 3412	-1.64	0.76	-5.08	-0.78	0.047	0.090	1.32	4.99	5.76	1.42	3.55	6.41	2.63	6.58	0.097	0.237	3.48	3.05	2.91	1.71	0.95	0.80	2.93	0.039	0.090	
±	0.12	0.05	0.10	0.07	0.006	0.006	0.10	0.12	0.17	0.11	0.12	0.02	0.09	0.54	0.002	0.004	0.13	0.08	0.07	0.03	0.05	0.04	0.03	0.003	0.001	
NGC 3414	-1.74	0.31	-6.30	-1.43	0.173	0.236	1.43	5.58	5.79	1.60	3.95	8.56	1.68	4.91	0.184	0.337	4.93	3.08	2.64	1.67	0.96	1.01	5.32	0.046	0.091	
±	0.20	0.16	0.19	0.13	0.005	0.007	0.08	0.17	0.12	0.15	0.08	0.23	0.12	0.25	0.003	0.003	0.10	0.07	0.06	0.08	0.04	0.11	0.02	0.001	0.003	
NGC 3599	0.88	1.75	-1.96	0.78	0.018	0.062	0.80	3.36	4.44	1.36	3.27	5.98	2.74	5.10	0.094	0.211	2.67	2.94	2.61	1.46	0.99	0.78	3.0			

Table B 1. Fully corrected Lick/IDS indices for the central  $r_*/8$  extraction: continued.

Galaxy	$H\delta_A$ [Å]	$H\delta_F$ [Å]	$H\gamma_A$ [Å]	$H\gamma_F$ [Å]	$CN_1$ [mag]	$CN_2$ [mag]	Ca4227 [Å]	G4300 [Å]	Fe4383 [Å]	Ca4455 [Å]	Fe4531 [Å]	C <sub>2</sub> 4668 [Å]	$H\beta$ [Å]	Fe5015 [Å]	Mg <sub>1</sub> [mag]	Mg <sub>2</sub> [mag]	Mg <sub>b</sub> [Å]	Fe5270 [Å]	Fe5335 [Å]	Fe5406 [Å]	Fe5709 [Å]	Fe5782 [Å]	NaD [Å]	TiO <sub>1</sub> [mag]	TiO <sub>2</sub> [mag]	
NGC 3613	-2.53	0.35	-5.82	-1.29	0.093	0.134	0.92	5.11	5.93	1.62	3.69	7.17	1.75	6.17	0.125	0.280	4.12	3.35	2.97	1.66	0.91	1.09	4.24	0.035	0.098	
±	0.27	0.12	0.19	0.11	0.003	0.002	0.13	0.11	0.19	0.14	0.11	0.18	0.10	0.21	0.002	0.000	0.06	0.08	0.13	0.08	0.05	0.11	0.13	0.003	0.001	
NGC 3636	-1.82	0.48	-5.95	-1.61	0.064	0.101	1.01	5.04	5.39	1.57	3.91	6.12	1.91	5.09	0.108	0.249	3.82	3.23	2.78	1.55	0.85	0.91	3.31	0.040	0.099	
±	0.41	0.14	0.11	0.21	0.004	0.005	0.16	0.29	0.27	0.15	0.20	0.09	0.11	0.34	0.003	0.002	0.10	0.16	0.16	0.07	0.21	0.29	0.16	0.004	0.002	
NGC 3640	-1.82	0.01	-5.55	-0.97	0.128	0.178	1.19	5.39	5.93	1.48	3.37	7.16	2.06	6.00	0.143	0.289	3.97	3.29	2.88	1.76	1.09	1.14	3.49	0.046	0.082	
±	0.26	0.13	0.18	0.07	0.025	0.032	0.14	0.34	0.16	0.09	0.16	0.31	0.12	0.17	0.002	0.001	0.08	0.06	0.08	0.04	0.09	0.09	0.06	0.003	0.002	
NGC 3665	-1.18	1.14	-4.87	-0.46	0.085	0.128	1.28	4.64	6.12	1.62	3.56	8.07	2.18	5.13	0.152	0.309	4.14	3.19	2.91	1.86	1.08	1.03	4.13	0.035	0.099	
±	0.12	0.11	0.17	0.13	0.004	0.003	0.08	0.05	0.10	0.13	0.06	0.21	0.10	0.11	0.003	0.005	0.06	0.11	0.31	0.03	0.12	0.07	0.16	0.002	0.002	
NGC 3923 45°	-1.87	0.81	-6.86	-1.87	0.116	0.155	1.15	5.14	6.22	1.63	4.41	8.18	1.92	6.34	0.147	0.319	4.54	3.33	3.54	2.05	0.90	0.91	5.80	0.051	0.126	
±	0.24	0.09	0.15	0.04	0.010	0.005	0.16	0.25	0.29	0.15	0.20	0.03	0.08	0.33	0.005	0.005	0.08	0.10	0.08	0.07	0.03	0.09	0.06	0.003	0.002	
NGC 3923 90°	-3.63	-0.65	-5.54	-1.45	0.145	0.191	1.72	4.77	6.10	1.39	3.96	8.28	1.71	5.40	0.151	0.312	4.67	3.93	3.03	2.04	—	—	—	—	—	—
±	0.38	0.21	0.69	0.03	0.016	0.016	0.26	0.22	0.76	0.10	0.34	0.27	0.16	0.24	0.003	0.001	0.14	0.15	0.55	0.04	—	—	—	—	—	—
NGC 3941	-2.20	0.62	-6.49	-1.55	0.093	0.134	1.08	5.51	6.28	1.74	3.67	7.65	2.02	5.44	0.117	0.276	4.12	3.22	3.01	1.72	1.05	1.01	3.80	0.035	0.094	
±	0.08	0.05	0.17	0.11	0.001	0.002	0.06	0.09	0.18	0.04	0.13	0.24	0.07	0.14	0.005	0.002	0.05	0.05	0.07	0.06	0.03	0.04	0.10	0.002	0.001	
NGC 4125	-1.75	0.26	-5.82	-1.09	0.126	0.182	1.35	5.35	6.52	1.96	3.60	7.77	1.76	5.64	0.162	0.310	3.96	3.39	2.79	1.98	1.07	0.84	4.89	0.045	0.082	
±	0.18	0.12	0.13	0.09	0.002	0.003	0.07	0.08	0.16	0.15	0.08	0.06	0.10	0.45	0.002	0.003	0.10	0.11	0.12	0.13	0.01	0.08	0.11	0.004	0.001	
NGC 4261	-2.79	0.07	-6.57	-1.78	0.140	0.189	1.34	4.94	6.64	1.72	3.78	9.12	1.41	4.45	0.163	0.336	5.11	3.31	3.12	1.81	0.91	1.05	5.93	0.034	0.117	
±	0.16	0.26	0.34	0.14	0.004	0.005	0.13	0.32	0.19	0.08	0.06	0.21	0.12	0.33	0.003	0.002	0.08	0.10	0.10	0.16	0.17	0.21	0.19	0.005	0.005	
NGC 4365	-3.28	-0.06	-6.55	-1.56	0.172	0.225	1.30	5.15	6.38	1.74	3.69	8.11	1.73	5.57	0.175	0.345	4.73	3.48	3.13	2.24	0.92	0.90	5.56	0.055	0.098	
±	0.18	0.12	0.13	0.06	0.007	0.005	0.06	0.06	0.23	0.08	0.13	0.07	0.12	0.10	0.001	0.002	0.07	0.03	0.14	0.04	0.09	0.04	0.18	0.002	0.003	
NGC 4374	-2.43	0.31	-6.05	-1.34	0.123	0.168	1.42	5.06	5.91	1.44	3.87	7.41	1.84	5.06	0.148	0.306	4.68	2.90	3.12	1.86	0.81	0.87	4.52	0.037	0.104	
±	0.27	0.13	0.14	0.17	0.005	0.003	0.05	0.09	0.14	0.07	0.14	0.11	0.11	0.23	0.001	0.001	0.06	0.12	0.18	0.09	0.07	0.06	0.09	0.002	0.003	
NGC 4494 0°	-1.02	0.65	-5.99	-1.49	0.103	0.157	1.13	5.31	5.41	1.63	4.28	7.98	1.77	6.11	0.137	0.275	3.90	3.09	2.68	1.68	0.94	0.89	3.93	0.042	0.080	
±	0.10	0.08	0.17	0.01	0.002	0.002	0.02	0.17	0.11	0.03	0.07	0.19	0.01	0.04	0.002	0.002	0.08	0.05	0.06	0.04	0.03	0.02	0.04	0.003	0.001	
NGC 4494 90°	—	—	—	—	—	—	—	—	—	—	—	—	—	—	—	—	—	—	—	—	—	—	—	—	—	
±	—	—	—	—	—	—	—	—	—	—	—	—	—	—	—	—	—	—	—	—	—	—	—	—	—	
NGC 4550	-0.02	1.93	-3.78	-0.40	-0.027	0.008	1.23	3.85	4.69	1.36	-0.05	4.64	2.24	4.03	0.079	0.213	3.44	2.83	2.80	1.43	1.02	0.69	2.88	0.026	0.075	
±	0.11	0.21	0.38	0.20	0.004	0.005	0.27	0.17	0.36	0.02	2.87	0.43	0.37	0.12	0.001	0.002	0.04	0.35	0.33	0.15	0.22	0.11	0.08	0.002	0.003	
NGC 4754	-3.23	0.12	-6.92	-1.87	0.135	0.181	1.42	5.35	6.60	1.81	3.90	9.01	1.59	6.40	0.178	0.357	4.60	3.73	3.40	1.86	0.86	0.87	4.52	0.042	0.103	
±	0.14	0.04	0.13	0.09	0.003	0.004	0.05	0.05	0.14	0.08	0.08	0.13	0.09	0.15	0.003	0.004	0.06	0.12	0.08	0.06	0.04	0.10	0.14	0.002	0.001	
NGC 5322	-0.96	0.76	-6.15	-1.44	0.103	0.161	1.37	5.36	6.04	1.80	3.72	8.27	2.08	6.03	0.149	0.301	4.16	3.42	2.90	1.98	1.03	1.18	4.36	0.043	0.083	
±	0.14	0.14	0.05	0.02	0.005	0.004	0.06	0.06	0.07	0.09	0.14	0.11	0.09	0.14	0.001	0.002	0.08	0.05	0.11	0.07	0.01	0.07	0.04	0.001	0.004	
NGC 5353	-1.23	0.50	-7.08	-1.93	0.159	0.212	1.31	5.15	6.48	1.93	3.96	10.31	1.68	6.24	0.201	0.371	5.18	3.73	3.55	1.81	0.81	1.13	6.74	0.058	0.101	
±	0.45	0.24	0.16	0.14	0.014	0.020	0.10	0.24	0.21	0.07	0.08	0.43	0.09	0.19	0.003	0.001	0.10	0.16	0.15	0.10	0.10	0.15	0.10	0.000	0.004	
NGC 5354 90°	-2.09	0.23	-6.30	-1.63	0.087	0.124	1.20	5.27	5.75	1.59	4.08	6.75	1.17	4.22	0.135	0.296	4.01	3.39	2.92	1.54	0.65	1.05	4.29	0.024	0.094	
±	0.25	0.33	0.18	0.18	0.013	0.013	0.20	0.30	0.05	0.14	0.23	0.17	0.51	0.005	0.009	0.21	0.06	0.11	0.07	0.12	0.08	0.13	0.005	0.004		
NGC 5354 0°	-1.65	0.39	-6.92	-1.91	0.095	0.146	1.18	5.36	5.95	1.36	3.71	8.04	1.56	5.17	0.166	0.320	4.59	3.19	3.01	2.17	0.94	0.88	4.81	0.045	0.090	
±	0.35	0.33	0.12	0.09	0.005	0.004	0.06	0.09	0.32	0.17	0.22	0.28	0.12	0.17	0.005	0.004	0.13	0.19	0.20	0.11	0.03	0.14	0.003	0.001		
NGC 5363	-2.02	-0.06	-5.31	-1.09	0.152	0.200	0.79	5.01	5.61	1.41	3.03	6.34	1.98	4.15	0.160	0.293	4.01	3.00	2.24	1.68	1.05	1.12	6.47	0.044	0.100	
±	0.42	0.24	0.25	0.15	0.018	0.016	0.23	0.12	0.18	0.08	0.10	0.40	0.19	0.20	0.005	0.007	0.19	0.11	0.15	0.07	0.05	0.04	0.11	0.002	0.001	
NGC 5444	-2.68	0.23	-6.60	-1.80	0.124	0.170	1.41	5.61	6.07	1.43	4.15	8.21	1.19	5.79	0.141	0.329	4.88	3.01	3.30	1.94	0.78	0.83	5.24	0.021	0.097	
±	0.12	0.11	0.43	0.14	0.009	0.010	0.17	0.34	0.24	0.12	0.25	0.44	0.09	0.16	0.002	0.005	0.07	0.13	0.05	0.06	0.10	0.14	0.22	0.005	0.001	
NGC 5557	-2.04	0.14	-5.93	-1.42	0.098	0.130	1.27	5.16	5.98	1.55	3.55	7.89	1.62	5.95	0.137	0.308	4.55									

Table B 1. Fully corrected Lick/IDS indices for the central  $z=8$  extraction: continued.

Galaxy	$H\delta_A$ [Å]	$H\delta_F$ [Å]	$H\gamma_A$ [Å]	$H\gamma_F$ [Å]	$CN_1$ [mag]	$CN_2$ [mag]	Ca4227 [Å]	G4300 [Å]	Fe4383 [Å]	Ca4455 [Å]	Fe4531 [Å]	$C_24668$ [Å]	$H\beta$ [Å]	Fe5015 [Å]	$Mg_1$ [mag]	$Mg_2$ [mag]	$Mg_b$ [Å]	Fe5270 [Å]	Fe5335 [Å]	Fe5406 [Å]	Fe5709 [Å]	Fe5782 [Å]	NaD [Å]	TiO <sub>1</sub> [mag]	TiO <sub>2</sub> [mag]			
NGC 5812	-2.34	-0.04	-6.97	-2.14	0.141	0.191	1.27	5.27	6.08	1.54	3.98	8.74	1.63	6.51	0.153	0.336	4.92	3.49	3.38	1.95	0.80	0.90	5.62	0.034	0.102			
±	0.11	0.10	0.44	0.49	0.005	0.004	0.07	0.21	0.32	0.11	0.12	0.22	0.06	0.10	0.003	0.002	0.13	0.05	0.05	0.07	0.07	0.03	0.09	0.003	0.003			
NGC 5813	-3.50	-0.07	-6.80	-2.17	0.085	0.119	1.59	5.70	5.81	1.81	4.05	8.07	1.58	4.69	—	—	4.64	3.01	2.67	1.85	0.81	1.09	4.63	0.047	0.096			
±	0.13	0.09	0.15	0.09	0.003	0.003	0.09	0.17	0.24	0.10	0.15	0.30	0.11	0.22	—	—	0.06	0.05	0.11	0.09	0.04	0.08	0.06	0.003	0.001			
NGC 5831	-2.48	0.55	-5.63	-1.28	0.117	0.160	1.19	4.75	6.19	1.52	3.87	7.97	1.47	5.94	0.158	0.328	4.58	3.42	3.27	1.69	0.96	0.97	4.44	0.036	0.105			
±	0.15	0.09	0.29	0.13	0.008	0.008	0.19	0.17	0.26	0.11	0.14	0.42	0.14	0.24	0.007	0.007	0.05	0.14	0.08	0.11	0.07	0.10	0.06	0.004	0.004			
NGC 5845	-2.65	0.05	-6.05	-1.57	0.140	0.197	1.48	5.59	5.60	1.77	3.99	7.48	1.93	5.65	0.175	0.330	4.56	3.37	3.23	1.88	1.03	0.89	4.79	0.045	0.083			
±	0.37	0.13	0.08	0.04	0.005	0.006	0.07	0.14	0.21	0.13	0.15	0.28	0.09	0.16	0.003	0.004	0.13	0.08	0.09	0.07	0.12	0.08	0.09	0.002	0.004			
NGC 5846 0°	-2.50	0.27	-7.03	-1.87	0.120	0.157	0.68	5.92	6.75	1.48	3.70	9.07	1.52	4.48	0.171	0.331	4.74	3.17	2.92	1.88	0.94	1.00	5.12	0.051	0.090			
±	0.30	0.21	0.24	0.12	0.023	0.026	0.23	0.16	0.20	0.10	0.12	0.37	0.11	0.12	0.002	0.007	0.05	0.11	0.17	0.04	0.03	0.04	0.08	0.002	0.003			
NGC 5846 90°	—	—	—	—	—	—	—	—	—	—	—	—	—	—	—	—	—	—	—	1.83	0.77	0.86	5.00	0.045	0.113			
±	—	—	—	—	—	—	—	—	—	—	—	—	—	—	—	—	—	—	—	0.14	0.07	0.07	0.14	0.002	0.001			
NGC 5846 A	-2.43	0.44	-5.91	-1.59	0.120	0.167	0.89	5.52	4.79	1.58	4.21	7.17	1.48	5.84	0.152	0.312	4.51	2.96	3.01	1.63	0.74	0.82	4.67	0.048	0.095			
±	0.25	0.37	0.13	0.17	0.024	0.029	0.24	0.20	0.26	0.21	0.34	0.45	0.17	0.33	0.008	0.004	0.24	0.17	0.33	0.11	0.09	0.02	0.07	0.001	0.004			
NGC 5854	—	—	—	—	—	—	—	—	—	—	—	—	—	—	—	—	—	—	—	2.50	2.20	1.23	1.02	0.73	0.39	2.69	0.033	0.083
±	—	—	—	—	—	—	—	—	—	—	—	—	—	—	—	—	—	—	—	0.17	0.14	0.09	0.11	0.10	0.06	0.003	0.003	
NGC 5864	-1.72	0.58	-5.03	-0.62	0.014	0.053	1.22	5.07	5.52	1.14	3.47	6.15	2.02	6.20	0.093	0.211	2.78	2.79	2.71	1.50	1.07	0.37	3.14	0.027	0.094			
±	0.18	0.23	0.14	0.16	0.007	0.005	0.13	0.22	0.29	0.08	0.25	0.20	0.09	0.42	0.002	0.002	0.15	0.15	0.13	0.08	0.11	0.11	0.05	0.004	0.004			
NGC 5869	—	—	—	—	—	—	—	—	—	—	—	—	—	—	—	—	—	—	—	1.88	0.80	1.02	4.25	0.033	0.107			
±	—	—	—	—	—	—	—	—	—	—	—	—	—	—	—	—	—	—	—	0.08	0.08	0.05	0.20	0.003	0.001			
NGC 5982	-2.04	0.27	-5.86	-1.37	0.099	0.142	1.40	5.24	5.86	1.78	3.75	8.99	1.47	5.88	0.129	0.300	4.44	3.16	3.04	1.76	0.66	1.14	4.96	0.034	0.102			
±	0.17	0.14	0.15	0.03	0.006	0.008	0.03	0.12	0.20	0.21	0.11	0.18	0.07	0.26	0.002	0.003	0.11	0.14	0.09	0.09	0.04	0.08	0.06	0.002	0.002			
NGC 6172	1.04	1.98	-3.31	-0.26	0.010	0.048	0.61	4.20	4.56	1.22	3.09	7.59	2.48	4.72	0.080	0.210	2.94	2.88	2.52	1.20	0.89	1.23	4.00	0.036	0.076			
±	0.17	0.15	0.20	0.21	0.005	0.005	0.06	0.12	0.31	0.11	0.09	0.25	0.15	0.37	0.009	0.008	0.11	0.11	0.10	0.07	0.04	0.05	0.07	0.003	0.005			
NGC 6411	-1.40	0.58	-6.18	-1.47	0.040	0.073	1.15	5.45	6.20	1.54	3.84	6.95	1.71	5.41	0.123	0.284	3.84	3.33	2.36	1.46	0.94	0.82	3.88	0.035	0.116			
±	0.27	0.17	0.13	0.09	0.010	0.006	0.05	0.17	0.41	0.14	0.15	0.22	0.01	0.38	0.002	0.004	0.05	0.10	0.17	0.05	0.05	0.05	0.10	0.002	0.002			
NGC 7302	-1.67	0.64	-5.62	-1.31	0.060	0.098	1.25	4.73	6.46	1.44	4.51	7.66	1.94	6.48	0.105	0.259	3.62	3.45	2.75	1.84	0.93	0.97	3.71	0.038	0.086			
±	0.61	0.14	0.28	0.20	0.025	0.033	0.11	0.37	0.13	0.21	0.52	0.20	0.10	0.20	0.002	0.003	0.18	0.10	0.16	0.09	0.06	0.07	0.09	0.002	0.006			
NGC 7332	-1.26	1.03	-5.09	-0.49	0.047	0.085	1.09	5.20	6.02	1.52	4.16	7.67	2.49	6.82	0.117	0.248	3.79	3.30	2.90	1.71	1.05	0.97	4.18	0.042	0.078			
±	0.13	0.11	0.07	0.04	0.008	0.009	0.06	0.19	0.27	0.03	0.34	1.12	0.26	0.10	0.008	0.011	0.10	0.06	0.05	0.05	0.04	0.03	0.004	0.003				
NGC 7454	-0.50	1.22	-4.66	-0.55	0.024	0.069	1.26	5.39	4.79	1.57	3.58	6.60	2.21	5.78	0.095	0.223	3.29	2.76	2.32	1.54	0.91	0.55	2.45	0.033	0.059			
±	0.51	0.33	0.13	0.08	0.011	0.013	0.13	0.16	0.22	0.12	0.22	0.50	0.13	0.28	0.005	0.002	0.04	0.08	0.09	0.08	0.08	0.08	0.09	0.001	0.003			
NGC 7585	1.36	2.02	-2.82	0.36	-0.018	0.032	1.10	3.90	5.57	1.66	3.57	6.84	2.65	5.27	0.108	0.256	3.45	3.08	2.58	1.66	0.83	1.11	4.29	0.032	0.068			
±	0.13	0.13	0.16	0.08	0.006	0.007	0.05	0.06	0.11	0.07	0.09	0.47	0.17	0.15	0.002	0.002	0.05	0.12	0.31	0.04	0.04	0.04	0.08	0.001	0.000			
NGC 7619	-3.40	-0.18	-6.89	-1.98	0.136	0.194	2.06	5.55	6.59	2.24	4.21	10.04	1.48	6.22	0.156	0.328	5.32	3.75	3.83	2.32	1.13	1.21	5.85	0.056	0.104			
±	0.09	0.08	0.11	0.06	0.006	0.007	0.13	0.10	0.12	0.17	0.13	0.19	0.09	0.19	0.002	0.001	0.07	0.06	0.11	0.06	0.05	0.05	0.04	0.003	0.005			
NGC 7626	-3.29	-0.16	-6.47	-1.83	0.131	0.187	1.48	4.95	5.54	1.89	3.41	8.77	1.33	5.83	0.156	0.335	5.07	3.20	3.42	1.92	0.94	1.19	5.74	0.048	0.107			
±	0.23	0.24	0.23	0.12	0.008	0.009	0.13	0.25	0.32	0.24	0.28	0.34	0.12	0.18	0.003	0.002	0.12	0.09	0.17	0.11	0.03	0.05	0.03	0.003	0.005			